

The First *Swift* Ultra-Violet/Optical Telescope GRB Afterglow Catalog

P. W. A. Roming¹, T. S. Koch¹, S. R. Oates², B. L. Porterfield³, D. E. Vanden Berk¹, P. T. Boyd⁴, S. T. Holland^{4,5,6}, E. A. Hoversten¹, S. Immler^{4,5}, F. E. Marshall⁴, M. J. Page², J. L. Racusin¹, D. P. Schneider¹, A. A. Breeveld², P. J. Brown¹, M. M. Chester¹, A. Cucchiara¹, M. De Pasquale², C. Gronwall¹, S. D. Hunsberger¹, N. P. M. Kuin², W. B. Landsman⁴, P. Schady², M. Still²

ABSTRACT

We present the first *Swift* Ultra-Violet/Optical Telescope (UVOT) gamma-ray burst (GRB) afterglow catalog. The catalog contains data from over 64,000 independent UVOT image observations of 229 GRBs first detected by *Swift*, the *High Energy Transient Explorer 2* (HETE2), the *INTErnational Gamma-Ray Astrophysics Laboratory* (INTEGRAL), and the Interplanetary Network (IPN). The catalog covers GRBs occurring during the period from 2005 Jan 17 to 2007 Jun 16 and includes $\sim 86\%$ of the bursts detected by the *Swift* Burst Alert Telescope (BAT). The catalog provides detailed burst positional, temporal, and photometric information extracted from each of the UVOT images. Positions for bursts detected at the 3σ -level are provided with a nominal accuracy, relative to the USNO-B1 catalog, of $\sim 0''.25$. Photometry for each burst is given in three UV bands, three optical bands, and a ‘white’ or open filter. Upper limits for magnitudes are reported for sources detected below 3σ . General properties of the burst sample and light curves, including the filter-dependent temporal slopes, are also provided. The majority of the UVOT light curves, for bursts detected at

¹Department of Astronomy & Astrophysics, Penn State University, 525 Davey Lab, University Park, PA 16802, USA; Corresponding author’s e-mail: roming@astro.psu.edu

²Mullard Space Science Laboratory, University College London, Holmbury St. Mary, Dorking, Surrey RH5 6NT, UK

³State College Area High School, 653 Westerly Parkway, State College, PA 16801, USA

⁴NASA/Goddard Space Flight Center, Greenbelt, MD 20771, USA

⁵Universities Space Research Association, 10227 Wincopin Circle, Suite 500, Columbia, MD 21044, USA

⁶Centre for Space Research in Space Science and Technology, Code 660, NASA/GSFC, 8800 Greenbelt Rd, Greenbelt, MD 20771, USA

the 3σ -level, can be fit by a single power-law, with a median temporal slope (α) of 0.96, beginning several hundred seconds after the burst trigger and ending at $\sim 1 \times 10^5$ s. The median UVOT v -band (~ 5500 Å) magnitude at 2000 s for a sample of “well” detected bursts is 18.02. The UVOT flux interpolated to 2000 s after the burst, shows relatively strong correlations with both the prompt *Swift* BAT fluence, and the *Swift* X-ray flux at 11 hours after the trigger.

Subject headings: catalogs — gamma-rays: bursts

1. Introduction

The Ultraviolet/Optical Telescope (UVOT; Roming et al. 2005) on board the *Swift* (Gehrels et al. 2004) observatory, provides rapid follow-up observations of GRB afterglows at UV and optical wavelengths. Typical times from a *Swift* Burst Alert Telescope (BAT; Barthelmy et al. 2005) GRB trigger to first UVOT observation range from 40 to 200 seconds. The UVOT usually provides the first optical, and almost always the only UV observations, of GRB afterglows. For detected GRB afterglows, the UVOT provides rapidly available sub-arcsecond locations, as well as high time resolution light curves in up to seven broad photometric bands. The relatively deep UVOT detection limits at early times also place constraints on the “dark burst” phenomenon (cf. Roming et al. 2006b). In addition, the UVOT observations are made simultaneously with X-ray observations with the coaligned *Swift* X-Ray Telescope (XRT; Burrows et al. 2005), allowing direct comparison of burst properties in X-ray and UV/optical light.

This paper describes the first *Swift* UVOT GRB afterglow catalog, containing information on bursts observed during the first 2.5 years of UVOT operation (2005-2007; corresponding to the instrument turn-on until the end of the 1st BAT GRB catalog (Sakamoto et al. 2007)). The catalog includes 205 bursts first detected by the *Swift* BAT, and 24 bursts first detected by other satellites or networks: the *High Energy Transient Explorer 2* (HETE2; Ricker 1997), the *INTErnational Gamma-Ray Astrophysics Laboratory* (INTEGRAL), and the Interplanetary Network (IPN; Hurley et al. 2005a). Information is provided for over 64,000 individual images of GRB fields taken by the UVOT.

In Section 2, we present the observations made by the UVOT. In Section 3, we describe the construction of the databases and the catalog. In Section 4, we describe the format of the databases and catalog. In Section 5, we provide a summary of the catalog. In Section 6 we summarize future work to be accomplished. The databases and catalog are provided in

electronic format with this paper and are also available at the *Swift* website¹.

2. Observations

The UVOT utilizes seven broadband filters during the observation of GRBs. The characteristics of the filters — central wavelength (λ_c), FWHM, zero points (the magnitudes at which the detector registers 1 counts s⁻¹; m_z), and the flux conversion factors (f_λ) — can be found in Table 1 (Poole et al. 2008; Roming et al. 2005). The flux density conversion factors are calculated based on model GRB power law spectra with a redshift ranging from $0.3 < z < 1.0$ (Poole et al. 2008)². The nominal image scale for UVOT images is 0''.502 pixel⁻¹ (unbinned). UVOT data is collected in one of two modes: event (or photon counting) and image. Event mode captures the time of the arriving photon as well as the celestial coordinates. The temporal resolution in this mode is ~ 11 ms. In image mode, photons are counted during the exposure and the position is recorded, but no timing information is stored except for the start and stop times of the exposure. Because the spacecraft has limited data storage capabilities, most UVOT observations are performed in image mode since the telemetry rate is significantly lower than event mode observations.

Since the launch of *Swift*, the automated observing sequence of the UVOT has been changed a few times in order to optimize observations of GRBs. The automated sequence is a set of variables which includes, but is not limited to, the filters, modes, and exposure times. The basic automated sequence design consists of finding charts and a series of short, medium, and long exposures in various filters. The finding charts are typically taken in both event and image mode simultaneously, in both the *white* and *v* filters, and have exposure times ranging from 100 – 400 s. A subset of these finding charts are immediately telemetered to ground-based telescopes to aid in localizing the GRB³. After completion of the *white* and *v* finding charts, a series of short exposures is typically taken in event mode, in all seven broadband filters, and has exposure times ranging from 10 – 50 s. A series of medium exposures is

¹http://swift.gsfc.nasa.gov/docs/swift/results/uvot_grbcats/

²The most recent calibration data are available from the *Swift* calibration database at <http://swift.gsfc.nasa.gov/docs/heasarc/caldb/swift/>

³A discussion of the finding chart and simultaneous observations in event and image mode is beyond the scope of this paper. The reader is referred to Roming et al. (2005). For observations between 2006 Jan 10 to 2006 Feb 13, and 2006 Mar 15 to the present, a second set of finding charts was included in the sequence. The second set of finding chart exposures are taken in the same way as the first set, except that exposures in the *white* filter are taken in image mode only.

then taken in image mode, in all seven broadband filters, and has exposure times ranging from 100 – 200 s. Finally, a series of long exposures is taken in image mode, in all seven broadband filters, and has typical exposure times of 900 s.⁴ In all cases, exposures can be cut short due to observing constraints.

This catalog covers UVOT observations of 229 GRB afterglows from 2005 Jan 17 to 2007 Jun 16. It includes bursts detected by *Swift* BAT, HETE2, INTEGRAL, IPN and observed by UVOT. A total of 211 BAT-detected bursts were observed by the UVOT (after instrument turn on) representing 93% of the BAT sample. Those that were not observed by the UVOT were either too close in angular distance to a bright (~ 6 mag) source, or occurred during UVOT engineering observations. Not included in the catalog are nine bursts first detected by BAT and INTEGRAL and observed by UVOT but with no afterglow position reported by the XRT or ground based observers (see Table 2). Inspection of the UVOT images reveals no obvious afterglows for these bursts.

Hereafter, we adopt the notation $F(\nu, t) \propto t^{-\alpha} \nu^{-\beta}$ for the afterglow flux density as a function of time, where ν is the frequency of the observed flux density, t is the time post trigger, β is the spectral index which is related to the photon index Γ ($\beta = \Gamma - 1$), and α is the temporal decay slope.

3. Construction of the Databases and Catalog

To provide a baseline for understanding the work described below, we define three words in the context of this catalog: database, catalog, and photometry pipeline. The database is the repository for all UVOT GRB data processed by the photometry pipeline. The catalog is the compilation of the top-level data from the UVOT database, as well as other sources (i.e. the BAT catalog (Sakamoto et al. 2007), the Gamma-ray burst Coordinate Network (GCN; Barthelmy et al. 1995, 1998) Circulars, etc.) that provides the primary characteristics of each burst. The photometry pipeline is the script that combines the required FTOOLS (with `uvotsource` performing the photometry) to produce the database and catalog. Below we describe the construction of the image and event databases, the catalog, and the requisite quality checks.

⁴Between 2005 Jan 17 to 2006 Jan 9 and between 2006 Feb 24 to 2006 Mar 14, exposures taken in uvw2, uvm2, and uvw1 were taken in event mode.

3.1. Image Database Construction

The UVOT GRB photometric image database is a collection of raw photometric measurements of UVOT images. The first step in constructing the database was to build an archive of UVOT GRB images. To ensure that all of our images and exposure maps benefited from consistent and up-to-date calibrations and processing, the *Swift* Data Center reprocessed the entire UVOT GRB image archive⁵. For example, images taken early in the mission did not benefit from MOD-8 pattern noise correction. All reprocessed images are now MOD-8 corrected. A number of images in our archive did not have a fine aspect correction applied; many of these images were recovered by running `uvotskycorr`. Lastly, we corrected a number of images which had improper OBJECT keywords.

We developed an IDL based image processing pipeline to perform aperture photometry on our archive of re-processed sky images. Figure 1 is a diagram of the UVOT `uvotphot` photometric pipeline software (Version 1.0). The heart of `uvotphot` is the *Swift* UVOT tool `uvotsource`. The pipeline used HEADAS Version 6.4 and the 2007 November UVOT CALDB. Photometry was performed on individual sky images using the curves of growth from the *Swift* CALDB for the aperture correction model. Upper limits were reported for sources $< 3\sigma$.

Figure 1 shows the additional inputs to the `uvotphot` pipeline software. The GRB information file contains the best reported source position and error estimate for each burst. In a small number of cases, we refined the positions to better center bursts in our source apertures. References for the best reported burst positions can be found in Table 8. Source region files specify a simple circular inclusion region of a given aperture size. Aperture photometry using a $3.0''$ radius aperture was performed for Version 1.0 of the database. Since a $5.0''$ radius aperture (containing $85.8 \pm 3.8\%$ of the PSF) was used for calibrating the UVOT, an aperture correction is applied to the data (Poole et al. 2008).

Background regions contain inclusion regions for background estimation and exclusion regions to mask out sources and/or features in each field. In most cases we use a standard annular inclusion region of inner and outer radii of $27''.5$ and $35''.0$ around each burst. To decrease the number of background region files required by our pipeline, we constructed composite region files to mask out sources and features in all bands. A small number of fields required non-standard region files. The background is calculated by taking the average background of all the pixels in the net background region. The region files (and postage stamp images) used in our processing can be found at the *Swift* website.

⁵Version HEA_06DEC2006_V6.1.1_SWIFT_REL2.6(BLD20)PATCHED3_14MAR2007 was used.

Sources within $15''$ of each burst, which may contaminate photometry in our source apertures, are listed in the `UvotSourceTable.fits` product. For each source we record its position and the measured magnitude in each filter. Source contamination is evidenced as a non-zero offset in the light curve data products.

UVOT images which suffer from other sources of contamination or degradation (not including nearby sources) have been identified. Image quality information is recorded as a series of “flags” which correspond to 1) bursts embedded in a large halo structure from nearby bright stars, 2) images where the burst was near the edge of the FoV, 3) images with charge trails in the source aperture, 4) images with diffraction spikes in the source aperture, 5) images which do not have fine aspect corrections, and 6) bursts embedded in crowded fields. Flags set to true (“T”) indicate images which are of poor quality. Images considered to be of low quality and have at least one quality flag raised also have the Quality Flag set to true (“T”).

For images that were generated from both image and event mode simultaneously (usually the finding charts are taken in this dual mode), the event mode data are excluded from the image database. A description of the event mode data can be found in Section 3.2 below.

3.2. Event Database Construction

For each GRB, the first orbit *v* and *white* event lists were obtained from the the Swift Data Center. Like the sky images, the event lists benefited from reprocessing using UVOT(20071106) and MIS(20080326) calibration and processing pipeline. The *v* and *white* are the only filters for which event lists have been included in the catalog because these filters are used for the finding chart exposures, which are expected to show variability on the shortest timescales.

The event processing pipeline is based on PERL and implements the *Swift* software and calibration found in the HEADAS 6.3.2 release. The pipeline refines the aspect of the event lists and then extracts the photometry. During the slew, immediately after the BAT trigger, the star tracker reports step-like changes in position to the attitude file. The first stage of the pipeline corrects the positions in the attitude file using `attjumpcorr` and then recomputes the positions of every photon in the event list using the corrected attitude file and the FTOOL `coordinator`. The pipeline then refines the aspect of the event list by creating images every 10 s and applying aspect correction software to each image. The aspect correction software locates the stars in each image and compares their positions to those in the USNO-B1 catalogue, correcting for proper motions. For each image, it computes

the RA and DEC offset between the stars in the image and those in the USNO-B1 catalogue. The offset is converted into pixels and then is applied to the position of each photon in the event list during the time interval of the image. To extract the photometry the pipeline runs `uvotevtlc` on the aspect corrected event lists using 10 s uniform binning, the 5" source regions and the background regions used to extract the image photometry.

The event lists, like the images, can suffer from a number of sources of contamination or degradation. These sources have been identified and flagged in a similar fashion as the UVOT images.

3.3. Catalog Construction

The UVOT GRB Catalog was constructed by combining information from various sources. Burst positions, trigger time, and time to the first UVOT observation were extracted from the image database. The magnitude of the first and peak detections were also determined for each filter. A value of “-99” indicates that no UVOT data was available, while a value of “99” indicates a $< 3\sigma$ detection.

Additional information in the catalog was gleaned from the literature. A reference to the best reported burst position is provided. Also included is a flag indicating which observatory discovered each burst. Galactic absorption and HI column density along the line of sight, T_{90} , redshift, GRB fluence in the 15 – 150 keV band, radio flux, and a flag to indicate detections in ground-based $R - K$ bands are provided for each burst. Temporal slopes are derived for bursts with a sufficient number of significant detections, from which magnitudes are computed at 2000 s (see Section 5).

3.4. Quality Control

To verify the quality of the data, the following checks were performed: photometric and astrometric stability of field stars, light curve production and investigation of previously detected and non-detected afterglows, comparison of photometry to previously published results, and visual examination of flagged images. A description of each quality check is found below.

The stability of photometric and astrometric measurements made by the pipeline were tested by applying the pipeline to stars, located in the UVOT GRB fields, which have reliable astrometric and photometric measurements from the Sloan Digital Sky Survey (SDSS; York et al. 2000) database. From this database 108 test stars in 32 GRB fields were se-

lected which were: within $2'$ of the GRB location, have magnitudes such that the stars are detectable in the UVOT images, and are detected at the 3σ -level. Since we can not select where GRBs are located, the field stars were not selected to be standard stars. However, obvious variable stars were rejected from the sample. Astrometric and photometric measurements were made of these stars in every UVOT image that covers their locations. Statistical characterization of the distributions of positions and count rates of the stars was done in order to quantitatively describe both the internal and absolute accuracy and precision of the pipeline measurements.

The mean position offsets in each band, relative to the USNO-B1 positions, defines the absolute accuracy of the astrometry. The USNO-B1 positions are used because the USNO-B1 catalog covers the entire sky and all UVOT positions are determined from this catalog⁶. The peak of the angular offset is $0''.31$, $0''.41$, $0''.31$, $0''.19$, $0''.22$, $0''.19$, and $0''.14$ for the *uvw2*, *uvm2*, *uvw1*, *u*, *b*, *v*, and *white* filters, respectively (cf. Figure 2). To determine the internal precision of the astrometry, we have calculated the Rayleigh scale parameter for the distributions of angular offsets from the mean stellar positions. A Rayleigh distribution holds if the offsets in RA and DEC are independent and normally distributed with the same standard deviation, which is then equivalent to the Rayleigh scale parameter. The internal astrometric precision (given by the Rayleigh scale parameter) of each of the UVOT bands is $0''.27$, $0''.28$, $0''.24$, $0''.22$, $0''.21$, $0''.21$, and $0''.17$ for the *uvw2*, *uvm2*, *uvw1*, *u*, *b*, *v*, and *white* bands respectively.

The mean count rates of the stars, converted to magnitudes on the Johnson system, is compared with the SDSS magnitudes transformed to the Johnson system, to define the absolute accuracy of the photometry. The conversions from SDSS and UVOT magnitudes to the Johnson system are based on work by Jester et al. (2005) and Poole et al. (2008), respectively. The average absolute photometric offset between the SDSS and UVOT ($\text{SDSS} - \text{UVOT}$) is $+0.076$ ($\sigma = 0.052$), $+0.010$ ($\sigma = 0.049$), and -0.068 ($\sigma = 0.027$) magnitudes (3σ confidence limit) for the *u*, *b*, and *v* filters, respectively (cf. Figure 3). The standard deviation of the mean count rates defines the internal precision of the photometry. The average standard deviation about the mean, over the nominal magnitude range of $13.8 - 20.7$ is 0.11 , 0.13 , and 0.09 mag for the *uvw2*, *uvm2*, and *uvw1* filters, respectively, and over the nominal magnitude range of $11.5 - 19.4$ is 0.06 , 0.05 , 0.06 , and 0.05 mag for the *u*, *b*, *v*, and *white* filters, respectively (cf. Figure 4).

We also compared the catalog entries to published values. In a small number of cases,

⁶It has been noted by Monet et al. (2003) that there is a systematic offset as large as $0''.25$ between the SDSS and USNO-B1 positions *after* correcting for proper motions.

no sources were detected in the database whereas the literature provides light curves for faint detections. This is because the photometry database is constructed with individual, not co-added, images. The UVOT burst database results were also compared against the following published results in order to perform a consistency check for the following detected burst afterglows: GRBs 060218 (Campana et al. 2006), 050525A (Blustin et al. 2006), 060313 (Roming et al. 2006a), 061007 (Schady et al. 2007), 050319 (Mason et al. 2006), 050318 (Still et al. 2005), 050603 (Grupe et al. 2006), 051117A (Goad et al. 2007a), 050801 (De Pasquale et al. 2007), 050730 (Perri et al. 2007), and 050802 (Oates et al. 2007). The comparison resulted in all the catalog data being consistent with the published data.

Images will still be in the UVOT catalog even if certain quality checks are not passed. Some of the bad aspect correction flags were determined by keywords in the image files themselves, while others were flagged by the `uvotphot` photometry pipeline. Below is a description of the checks performed on all flagged images.

Settling: When the spacecraft reaches the target location, it requires a brief period of time to lock onto the target; this period is known as settling. During this time the UVOT is observing in event mode, typically in the *v*-filter. Because the UVOT detector voltage is changing during this period, the count rate is not calibrated; therefore, these images are flagged as settling exposures and should be used with caution. The criteria for flagging an image as a settling exposure is if the image is: the first in the first observation sequence, taken in event mode, taken in the *v*-filter, and the exposure time is < 11 s.

Each GRB observation for which the first finding chart exposure is present should include a settling exposure just prior to the start of the observation. This condition was checked in the database file, and cases where no settling image was flagged were investigated; this ensures that all settling images are flagged as such. To ensure that non-settling images have not been erroneously flagged, any settling mode images that were found to occur *after* the initial finding chart exposure were also investigated.

Aspect Correction: A small number of images which have a successful fine aspect correction are blurred due to uncorrected movement of the spacecraft. These images have been flagged.

Charge Trailing or In Halo: A subset of the database have been generated by filtering for anything flagged as “charge trailing” or “in halo.” Individual fields from this list were visually inspected to verify the condition. A random check in individual fields was also made in order to check for the existence of these conditions in cases where they were not flagged.

Edge Effect or Crowded Field: Some images are not well centered on the burst and suffer from “edge effects”, while other bursts are embedded in crowded star fields. These images

were flagged.

Near Bright Star: Co-added images in *b* and *uvw1* from the initial snapshot in each field were visually examined to search for nearby bright stars. Nearby bright stars with diffraction spikes impinging on the source aperture were flagged.

Cumulative Quality: If any of the quality flags above are set to true (“T”) this flag is also set to true. These images should be treated with caution when used in a dataset. Approximately 10% of all images are flagged. The largest contribution to flagged images are a result of in halo and charge trailing, totaling $\sim 6.2\%$ and $\sim 1.3\%$ of the images, respectively.

4. Database and Catalog Formats

The *Swift* UVOT Image Mode Burst Database (sample columns and rows are provided in Table 3), the *Swift* UVOT Event Mode Burst Database (sample columns and rows are provided in Table 4), and the *Swift* UVOT Burst Catalog (sample columns and rows provided in Table 5) can be found at the *Swift* website. The databases and catalog are available in the following file formats: (1) a standard ASCII file with fixed column widths (size = 12.3 MB, 521 kB, & 21 kB for the image and event databases, and the catalog, respectively) and (2) a binary FITS table (size = 13.9 MB, 560 kB, & 28 kB for the image and event databases, and the catalog, respectively).

The Image Mode Database contains 86 columns and 63,315 rows. Each column is described in Table 6. Except for the object ID, time of burst trigger, filter, quality flags, name of the FITS extension, trigger number, and filename in columns 1, 6, 12, and 76-86, all entries are in floating point, exponential, or integer format.

The Event Mode Database contains 41 columns and 9402 rows. Each column is described in Table 7. Except for the object ID, time of burst trigger, filter, quality flags, trigger number, and filename in columns 1, 6, 12, and 38-41, all entries are in floating point, exponential, or integer format.

The Burst Catalog contains 81 columns and 229 rows. Each column is described in Table 8. Except for the object ID, position reference, time of burst trigger, detection flags, and the notes in columns 1, 5, 9, and 78-81, respectively, all entries are in floating point, exponential, or integer format.

Below are the notes on the image database columns found in Table 6. Each note identifies the nomenclature and description of each column.

1. OBJECT: The object identification. The format is GRByymmddX, where *yy* is the last two digits of the year of the burst, *mm* is the month, *dd* is the day (in UTC), and *X* is used to represent a second, third, fourth, etc., burst occurring on a given day by the letters ‘B’ or ‘C’. Only the last seven characters are listed in the catalog (i.e. the “GRB” is dropped from each entry).

2. RA: The best J2000.0 right ascension, in decimal degrees, as found in the GCN Circulars⁷, Goad et al. (2007b), and Butler (2007). Thirteen GRBs have improved positions that were calculated from the centroid of the summed images in the UVOT image database; these have been identified in column 81 of the catalog.

3. DEC: The best J2000.0 declination, in decimal degrees, as described in RA above.

4. POS_ERR: Positional uncertainty, in arcseconds, as described in RA above.

5. TRIGTIME: The time of the burst trigger as measured in *Swift* mission elapsed time (MET). MET is measured in seconds and starts on 2001 January 1, 00:00:00.000 (UTC). The MET of the launch of *Swift*, 2004 November 20, 18:35:45.865 (UTC), is 122668545.865.

6. TRIG_UT: The time of the burst trigger as measured in Universal time (UTC) (e.g. 2005-017-12:52:36).

7. TIME: TSTART + TELAPSE/2 (see columns 8 & 11).

8. TSTART: The MET start time of the exposure.

9. TSTOP: The MET stop time of the exposure.

10. EXPOSURE: The exposure time, in seconds, including the following corrections: detector dead time, time lost when the on-board shift-and-add algorithm tosses event data off the image, time lost when the UVOT Digital Processing Unit stalls because of high count rates, and time lost due to exposures beginning with the UVOT blocked filter.

11. TELAPSE: TSTOP - TSTART, in seconds.

12. FILTER: The UVOT filter used for the exposure (uvw2, uvm2, uvw1, *u*, *b*, *v*, and *white*).

13. BINNING: The binning factor ($1 = 1 \times 1$ binning and $2 = 2 \times 2$ binning).

14. APERTURE: The source aperture radius, in arcseconds.

⁷http://gcn.gsfc.nasa.gov/gcn3_archive.html

15. SRC_AREA: The area of the source region, in square arcseconds, computed by multiplying the number of pixels found by XIMAGE within the source radius by the area of each pixel. This value can differ from the specified area πr^2 by up to 2% because XIMAGE selects whole pixels within the source radius. This approach produces an area slightly larger or smaller than πr^2 . Simulations reveal that the 1σ difference between the exact and XIMAGE areas are 1.0% and 1.5% for a 10 and 6 pixel radius, respectively. The error in photometry is much less than these area fluctuations because source counts are concentrated in the center of the aperture and the aperture correction uses the radius corresponding to the XIMAGE area.

16. BKG_AREA: The area, in square arcseconds, of the background region. It is calculated by taking the number of pixels in the background annulus and multiplying by the area of each pixel. Masked regions are excluded therefore only net pixels are included. This differs slightly from the exact area $\pi(r_o - r_i)^2$, but we are only interested in the background surface brightness, so the difference is not significant.

17. PLATE_SCALE: The plate scale, in arcseconds per pixel, of the image. The error in the mean plate scale is $\pm 0''.0005 \text{ pixel}^{-1}$.

18. RAW_TOT_CNTS: Total number of counts measured within the source region.

19. RAW_TOT_CNTS_ERR: The binomial error in RAW_TOT_CNTS. The binomial error is given by $(\text{RAW_TOT_CNTS})^{1/2} * ((\text{NFRAME} - \text{RAW_TOT_CNTS})/\text{NFRAME})^{1/2}$. $\text{NFRAME} = \text{TELAPSE} / \text{FRAMETIME}$, where $\text{FRAMETIME} = 0.011032 \text{ s}$ for the full FoV. NFRAME is the number of CCD frames (typically one every $\sim 11 \text{ ms}$). A discussion of the measurement errors in the UVOT can be found in Kuin & Rosen (2008).

20. RAW_BKG_CNTS: Total number of counts measured in the background annulus.

21. RAW_BKG_CNTS_ERR: The binomial error in RAW_BKG_CNTS. The binomial error is given by $(\text{RAW_BKG_CNTS})^{1/2} * ((\text{NFRAME} - \text{EFF_BKG_CNTS})/\text{NFRAME})^{1/2}$. $\text{EFF_BKG_CNTS} = \text{RAW_BKG_CNTS} * 80 / \text{BKG_AREA}$. The effective counts in the background (EFF_BKG_CNTS) is calculated because the background area is larger than the coincidence region. The value 80 is the area (in square arcseconds) of our circular aperture with a radius of $5''$.

22. RAW_STD_CNTS: Total number of counts measured within the standard $5''$ aperture. This constant value is based on the size of the current calibration aperture.

23. RAW_STD_CNTS_ERR: Binomial error associated with RAW_STD_CNTS.

24. RAW_TOT_RATE: The total measured count rate, in counts per second, in the

source region. Calculated using $\text{RAW_TOT_CNTS} / \text{EXPOSURE}$.

25. RAW_TOT_RATE_ERR : $\text{RAW_TOT_CNTS_ERR} / \text{EXPOSURE}$.

26. RAW_BKG_RATE : The total measured count rate, in counts per second per square arcsecond, in the background region. Calculated using $\text{RAW_BKG_CNTS} / \text{EXPOSURE} / \text{BKG_AREA}$.

27. RAW_BKG_RATE_ERR : $\text{RAW_BKG_CNTS_ERR} / \text{EXPOSURE} / \text{BKG_AREA}$.

28. GLOB_BKG_RATE : The global background rate, in counts per second per square arcsecond. The global background of each image is modeled as a Gaussian distribution. An iterative “Sigma Clipping” is performed to eliminate contributions from field stars above the 3σ level. The global background is then reported as the arithmetic mean of the clipped distribution along with the number of samples in the clipped distribution. In images where the background is well sampled, the ratio of local to global background rates is a good indicator of sources embedded in the halo of a nearby bright star.

29. GLOB_BKG_AREA : The area, in square arcseconds, of the global background region.

30. RAW_STD_RATE : The total measured count rate, in counts per second, in the coincidence loss region. Calculated using $\text{RAW_STD_CNTS} / \text{EXPOSURE}$.

31. RAW_STD_RATE_ERR : $\text{RAW_STD_CNTS_ERR} / \text{EXPOSURE}$.

32. COLSTD_FACTOR : The coincidence-loss correction factor for the coincidence-loss region. This is calculated as follows. First, the COLSTD_RATE (which is not recorded) is calculated using the theoretical coincidence loss formula and the polynomial correction to $\text{RAW_STD_RATE} = \text{RAW_STD_CNTS} / \text{EXPOSURE}$ (see eq. 1-3 in Poole et al. 2008). The value COLSTD_FACTOR is then the ratio $\text{COLSTD_RATE} / \text{RAW_STD_RATE}$.

33. COLSTD_FACTOR_ERR : The uncertainty in the coincidence correction (see eq. 4 in Poole et al. 2008).

34. COLBKG_FACTOR : The coincidence-loss correction factor for the background region.

35. COLBKG_FACTOR_ERR : The uncertainty in the coincidence correction of the background counts within the source aperture.

36. COLSRC_CNTS : The coincidence-loss corrected counts in the source region. Calculated using $(\text{RAW_TOT_CNTS} - (\text{RAW_BKG_CNTS} * \text{SRC_AREA} / \text{BKG_AREA})) * \text{COLSTD_FACTOR}$.

37. COL_SRC_CNTS_ERR: The error associated with COL_SRC_CNTS. Calculated using $(\text{RAW_TOT_CNTS_ERR} - (\text{RAW_BKG_CNTS_ERR} * \text{SRC_AREA} / \text{BKG_AREA})) * \text{COLSTD_FACTOR_ERR}$.

38. COL_BKG_CNTS: The coincidence-loss corrected counts in the background region. Calculated using $\text{RAW_BKG_CNTS} * \text{COL_BKG_FACTOR}$.

39. COL_BKG_CNTS_ERR: The error associated with COL_BKG_CNTS. Calculated using $\text{RAW_BKG_CNTS_ERR} * \text{COL_BKG_FACTOR_ERR}$.

40. COL_TOT_RATE: The coincidence-loss corrected raw count rate, in counts per second, in the source region. Calculated using $\text{RAW_TOT_RATE} * \text{COLSTD_FACTOR}$.

41. COL_TOT_RATE_ERR: Error in the $\text{COL_TOT_RATE} = \text{RAW_TOT_RATE_ERR} * \text{COLSTD_FACTOR}$.

42. COL_BKG_RATE: The coincidence-loss corrected background surface count rate, in counts per second per square arcsecond. Calculated using $\text{RAW_BKG_RATE} * \text{COL_BKG_FACTOR}$.

43. COL_BKG_RATE_ERR: Error in coincidence corrected background surface brightness. Calculates using $\text{RAW_BKG_RATE_ERR} * \text{COL_BKG_FACTOR}$.

44. COL_SRC_RATE: Coincidence corrected net count rate, in counts per second. Calculated using $\text{COL_TOT_RATE} - \text{COL_BKG_RATE} * \text{SRC_AREA}$.

45. COL_SRC_RATE_ERR: Error in the coincidence corrected net count rate. The errors in the source rate and the background rate are added in quadrature: $(\text{COL_TOT_RATE_ERR}^2 + (\text{COL_BKG_RATE_ERR} * \text{SRC_AREA})^2)^{1/2}$.

46. AP_FACTOR: Aperture correction for going from a 3'' radius to a 5'' radius aperture for the v filter. This is computed using the PSF stored in the CALDB by `uvotapercorr`. This is always set to 1.0 unless the `CURVEOFGROWTH` method is used. The source radius is defined to be $(\text{SRC_AREA} / \pi)^{1/2}$, so that one uses an effective source radius to the actual pixel area used by XIMAGE.

47. AP_FACTOR_ERR: The 1σ error in AP_FACTOR. $\text{AP_FACTOR_ERR} = \text{AP_COL_SRC_RATE_ERR} / \text{COL_SRC_RATE_ERR}$.

48. AP_SRC_RATE: Final aperture and coincidence loss corrected count rate used to derive the flux and magnitudes. Calculated using $\text{AP_FACTOR} * \text{COL_SRC_RATE}$.

49. AP_SRC_RATE_ERR: Error on the final count rate. Calculated using $(\text{COL_SRC_RATE_ERR}^2 + (\text{fwhmsig} * \text{COL_SRC_RATE})^2)^{1/2}$. The “fwhmsig” parameter is

the fractional RMS variation of the PSF which is set to $3''$. This variation is propagated through the uncertainty calculation, and is added in quadrature to the corrected measurement uncertainty.

50. MAG: The magnitude of the source in the UVOT system computed from AP_COI_SRC_RATE. The value is set to 99.00 for upper-limits.

51. MAG_ERR: The one-sigma error in MAG. Unless otherwise specified, all errors are the 1-sigma statistical errors based on Poisson statistics. The value is set to 9.90E+01 if MAG was an upper limit.

52. SNR: Signal-to-noise ratio calculated from COI_TOT_RATE and COI_BKG_RATE.

53. MAG_BKG: The sky magnitude, in magnitudes per square arcsecond, in the UVOT system computed from COI_BKG_RATE.

54. MAG_BKG_ERR: The one-sigma error in MAG_BKG.

55. MAG_LIM: The “N”-sigma limiting magnitude in the UVOT system computed from the RAW quantities.

56. MAG_LIM_SIG: “N” for MAG_LIM, where “N” is a chosen parameter. The database uses a value of 3 for N.

57. MAG_COLLIM: The magnitude at which the count rate is one count per CCD frame.

58. FLUX_AA: The flux density in $\text{erg s}^{-1} \text{cm}^{-2} \text{\AA}^{-1}$.

59. FLUX_AA_ERR: The one-sigma error in FLUX_AA.

60. FLUX_AA_BKG: The flux density of the sky in $\text{erg s}^{-1} \text{cm}^{-2} \text{\AA}^{-1}$ per square arcsecond.

61. FLUX_AA_BKG_ERR: The one-sigma error in FLUX_AA_BKG.

62. FLUX_AA_LIM: The approximate flux density limit based on an average GRB spectrum, in $\text{erg s}^{-1} \text{cm}^{-2} \text{\AA}^{-1}$.

63. FLUX_AA_COLLIM: The flux density at which the count rate is one count per frame time, in $\text{erg s}^{-1} \text{cm}^{-2} \text{\AA}^{-1}$.

64. FLUX_HZ: The flux density in mJy.

65. FLUX_HZ_ERR: The one-sigma error in FLUX_HZ.

66. FLUX_HZ_BKG: The flux density of the sky in mJy per square arcsecond.

67. `FLUX_HZ_BKG_ERR`: The one-sigma error in `FLUX_HZ_BKG`.
68. `FLUX_HZ_LIM`: The “N”-sigma limiting flux density in mJy, corresponding to `MAG_LIM`.
69. `FLUX_HZ_COI_LIM`: The flux density at which the count rate is one count per frame time, in mJy.
70. `NEAREST_RA`: The J2000.0 right ascension, in decimal degrees, of the closest non-GRB source within 15'' to the burst position, as determined by `uvotdetect`.
71. `NEAREST_DEC`: The J2000.0 declination, in decimal degrees, of the closest non-GRB source within 15'' to the burst position, as determined by `uvotdetect`.
72. `NEAREST_MAG`: The magnitude, in the given UVOT band, of the object at `CLS_SRC_RA` and `CLS_SRC_DEC`, as determined by `uvotdetect`. If there is no source found within 15'' radius of the burst position then this value is set to 99.00.
73. `CENTR_RA`: The source’s centroided right ascension, in decimal degrees, as determined by a 2D gaussian fit of the UVOT data. If the fit failed then the value is set to 999.000000.
74. `CENTR_DEC`: The source’s centroided declination, in decimal degrees, as determined by a 2D gaussian fit of the UVOT data. If the fit failed then the value is set to 999.000000.
75. `CENTR_ERR`: The larger of the fit errors between `CENTR_RA` and `CENTR_DEC` divided by the square-root of the number of counts (N). Given as a 1σ error. If the fit failed, then a value of -1.0 is assigned. $N = \text{MAX}(1, \text{RAW_TOT_CNTS} - [\text{RAW_BKG_RATE} * \text{EXPOSURE} * \text{SRC_AREA}])$.
76. `SETTLE_FLAG`: Settling images sometimes have a poor aspect solution which creates doublets out of field stars. Settling images also suffer from detector gain issues because the High Voltages may still be ramping up part way into the exposure. Such images have an undefined photometric calibration and should be used cautiously. Images fitting all of the following are flagged as settling exposures, i.e. this flag is true (T): first exposure of Segment 0, image taken in Event mode, and $\text{EXPOSURE} < 11$ s.
77. `ASPECT_FLAG`: The *Swift* spacecraft pointing accuracy is $\approx 5''$. The astrometric error is improved to about $0''.3$ by comparing source positions to the USNO-B catalog. For a small number of images the automated procedure did not produce an aspect solution. Such images are flagged as true (T).

78. TRAIL_FLAG: A number of *v* and *white* images suffer from the effects of charge trailing. This happens when bright sources align with the source aperture in the CCD readout direction. Visible bright streaks along CCD columns (RAWY) sometimes complicate photometric measurements. These images are flagged true (T).

79. CROWDED_FLAG: If the field appears crowded upon visual inspection the image is flagged true (T).

80. SPIKE_FLAG: If a diffraction spike impinges upon the source region then the image is flagged true (T).

81. EDGE_FLAG: If the source is sufficiently close to the edge of the image such that the exposure across the background region is variable then the image is flagged true (T).

82. HALO_FLAG: A few bursts lie within the halo of bright stars, which can produce erroneous photometric measurements. Such situations are flagged by comparing the local background to the global background. These images are flagged true (T).

83. QUALITY_FLAG: Cumulative quality flag. This flag is set to true (T) when any of the following quality flags are true (T): SETTLE_FLAG, ASPECT_FLAG, TRAIL_FLAG, SPIKE_FLAG, EDGE_FLAG, or HALO_FLAG.

84. TRIG_NUM: The *Swift* triggering number for the burst.

85. EXTNAME: The name of the FITS extension that contains this observation. The name of the extension has the following format: {filter}{exposure ID}{I/E} where {filter} = wh, vv, bb, uu, w1, m2, or w2 for the *white*, *v*, *b*, *u*, uvw1, uvm2, and uvw2, respectively, and {I/E} represents image or event mode (e.g. vv133535746I).

86. IMAGE_NAME: Name of the image (e.g. 00020004001/uvot/image/st00020004001ubb_sk.img.gz[1]).

Below are the notes on the event database columns found in Table 7. Each note identifies the nomenclature and description of each column.

1-17. OBJECT, RA, DEC, POS_ERR, TRIGTIME, TRIG_UT, TIME, TSTART, TSTOP, EXPOSURE, TELAPSE, FILTER, BINNING, APERTURE, SRC_AREA, BKG_AREA, & PLATE_SCALE: Same as columns 1-17 in Table 6, respectively.

18-21. COLSTD_FACTOR, COLSTD_FACTOR_ERR, COLBKG_FACTOR, & COLBKG_FACTOR_ERR: Same as columns 32-35 in Table 6, respectively.

22-28. COL_TOT_RATE, COL_TOT_RATE_ERR, COL_BKG_RATE, COL_BKG_RATE_ERR, COL_SRC_RATE, COL_SRC_RATE_ERR⁸, & AP_FACTOR: Same as columns 40-46 in Table 6, respectively.

29-32. AP_SRC_RATE, AP_SRC_RATE_ERR, MAG, & MAG_ERR: Same as columns 48-51 in Table 6, respectively.

33-34. FLUX_AA & FLUX_AA_ERR: Same as column 58-59 in Table 6, respectively.

35-39. CENTR_RA, CENTR_DEC, CENTR_ERR, SETTLE_FLAG, ASPECT_FLAG: Same as columns 73-77 in Table 6, respectively.

40-41. TRIG_NUM & FILENAME: Same as column 85-86 in Table 6.

Notes on the *Swift* UVOT burst catalog columns found in Table 8:

1-4. OBJECT, RA, DEC, & PNT_ERR: Same as columns 1-4 in Table 6, respectively.

5. POS_REF: The position reference for columns 2-4. References are from the the GCN Circulars, Goad et al. (2007b), and Butler (2007).

6. DISC_BY: The “discovery flag” indicating which spacecraft discovered the GRB. The flag is an integer from 0-2 representing: 0 = *Swift*, 1 = HETE2, 2 = INTEGRAL, and 3 = IPN.

7. T90: T_{90} , in seconds, as defined by Sakamoto et al. (2007) for the *Swift* discovered bursts in the 15 – 350 keV band. For GRBs 050408 (Sakamoto et al. 2005), 051021 (Olive et al. 2005), 051028 (Hurley et al. 2005b), 051211A (Kawai et al. 2005), and 060121 (Arimoto et al. 2005) discovered by HETE2, T_{90} in the 30 – 400 keV band is provided as in the GCN Circulars (T_{90} for GRB 060121 is provided in the 80 – 400 keV band). T_{90} for the INTEGRAL and IPN discovered bursts, as well as the remaining HETE2 bursts, were not available in the GCN Circulars. In all cases where T_{90} was not available this value is set to –99.0.

8-9. TRIGTIME & TRIG_UT: Same as columns 5 and 6 from Table 6, respectively.

10. FRST_TSTART: The start time of the first UVOT observation measured in seconds

⁸The values for COL_SRC_RATE_ERR & AP_SRC_RATE_ERR are not calculated correctly by the pipeline software and are therefore too large. These values will be corrected in future versions of the database.

from the burst trigger.

11. FRST_W2: The first reported magnitude in the uvw2-filter. If no detections are reported then this value is set to 99.00. If not observed in the uvw2-filter then this value is set to -99.00 .

12. FRST_W2_T: The time since burst, in seconds, to the middle of the exposure of FRST_W2. If $\text{FRST_W2} = \pm 99.00$ then this value is set to -1.0 .

13. FRST_M2: Same as FRST_W2 except for the uvm2-filter.

14. FRST_M2_T: The same as FRST_W2_T except for the uvm2-filter.

15. FRST_W1: Same as FRST_W2 except for the uvw1-filter.

16. FRST_W1_T: The same as FRST_W2_T except for the uvw1-filter.

17. FRST_UU: Same as FRST_W2 except for the u -filter.

18. FRST_UU_T: The same as FRST_W2_T except for the u -filter.

19. FRST_BB: Same as FRST_W2 except for the b -filter.

20. FRST_BB_T: The same as FRST_W2_T except for the b -filter.

21. FRST_VV: Same as FRST_W2 except for the v -filter.

22. FRST_VV_T: The same as FRST_W2_T except for the v -filter.

23. FRST_WH: Same as FRST_W2 except for the *white*-filter.

24. FRST_WH_T: The same as FRST_W2_T except for the *white*-filter.

25. PEAK_W2: The peak reported magnitude in the uvw2-filter. If no detections are reported then this value is set to 99.00. If not observed in the uvw2-filter then this value is set to -99.00 .

26. PEAK_W2_T: The time since burst, in seconds, to the middle of the exposure of PEAK_W2. If $\text{PEAK_W2} = \pm 99.00$ then this value is set to -1.0 .

27. PEAK_M2: Same as PEAK_W2 except for the uvm2-filter.

28. PEAK_M2_T: The same as PEAK_W2_T except for the uvm2-filter.

29. PEAK_W1: Same as PEAK_W2 except for the uvw1-filter.

30. PEAK_W1_T: The same as PEAK_W2_T except for the uvw1-filter.

31. PEAK_UU: Same as PEAK_W2 except for the u -filter.

- 32. PEAK_UU_T: The same as PEAK_W2_T except for the *u*-filter.
- 33. PEAK_BB: Same as PEAK_W2 except for the *b*-filter.
- 34. PEAK_BB_T: The same as PEAK_W2_T except for the *b*-filter.
- 35. PEAK_VV: Same as PEAK_W2 except for the *v*-filter.
- 36. PEAK_VV_T: The same as PEAK_W2_T except for the *v*-filter.
- 37. PEAK_WH: Same as PEAK_W2 except for the *white*-filter.
- 38. PEAK_WH_T: The same as PEAK_W2_T except for the *white*-filter.

39. ALPHA_W2: In the case of two or more afterglow detections in the uvw2-filter for a given burst, all occurring between $\sim 300 - 100,000$ s, the temporal slope (α_{uvw2}) for that filter is provided. If two or more detections are not found for any given segment, the value is set to -99.99 . The value is calculated using,

$$f_{\lambda(uvw2)} = At^{-\alpha_{uvw2}}, \quad (1)$$

where $f_{\lambda(uvw2)}$ is the flux density, A is the amplitude, and t is the time since burst.

40. ALPHA_W2_ERR: The one-sigma error in ALPHA_W2. If ALPHA_W2 = -99.99 then ALPHA_W2_ERR = -99.99 .

41. ALPHA_W2_AMP: The amplitude of ALPHA_W2. If ALPHA_W2 = -99.99 then ALPHA_AMP = -99.99 .

42. MAG_ALPHA_W2: The computed uvw2-filter magnitude at 2000 s derived from using ALPHA_W2. If ALPHA_W2 = -99.99 then MAG_ALPHA_W2 = -99.99 .

43. ALPHA_M2: Same as ALPHA_W2 except for the uvm2-filter.

44. ALPHA_M2_ERR: Same as ALPHA_W2_ERR except for the uvm2-filter.

45. ALPHA_M2_AMP: Same as ALPHA_W2_AMP except for the uvm2-filter.

46. MAG_ALPHA_M2: Same as MAG_ALPHA_W2 except for the uvm2-filter.

47. ALPHA_W1: Same as ALPHA_W2 except for the uvw1-filter.

48. ALPHA_W1_ERR: Same as ALPHA_W2_ERR except for the uvw1-filter.

49. ALPHA_W1_AMP: Same as ALPHA_W2_AMP except for the uvw1-filter.

50. MAG_ALPHA_W1: Same as MAG_ALPHA_W2 except for the uvw1-filter.

51. ALPHA_UU: Same as ALPHA_W2 except for the *u*-filter.

- 52. ALPHA_UU_ERR: Same as ALPHA_W2_ERR except for the *u*-filter.
- 53. ALPHA_UU_AMP: Same as ALPHA_W2_AMP except for the *u*-filter.
- 54. MAG_ALPHA_UU: Same as MAG_ALPHA_W2 except for the *u*-filter.
- 55. ALPHA_BB: Same as ALPHA_W2 except for the *b*-filter.
- 56. ALPHA_BB_ERR: Same as ALPHA_W2_ERR except for the *b*-filter.
- 57. ALPHA_BB_AMP: Same as ALPHA_W2_AMP except for the *b*-filter.
- 58. MAG_ALPHA_BB: Same as MAG_ALPHA_W2 except for the *b*-filter.
- 59. ALPHA_VV: Same as ALPHA_W2 except for the *v*-filter.
- 60. ALPHA_VV_ERR: Same as ALPHA_W2_ERR except for the *v*-filter.
- 61. ALPHA_VV_AMP: Same as ALPHA_W2_AMP except for the *v*-filter.
- 62. MAG_ALPHA_VV: Same as MAG_ALPHA_W2 except for the *v*-filter.
- 63. ALPHA_WH: Same as ALPHA_W2 except for the *white*-filter.
- 64. ALPHA_WH_ERR: Same as ALPHA_W2_ERR except for the *white*-filter.
- 65. ALPHA_WH_AMP: Same as ALPHA_W2_AMP except for the *white*-filter.
- 66. MAG_ALPHA_WH: Same as MAG_ALPHA_W2 except for the *white*-filter.
- 67. BBMINUSVV: MAG_ALPHA_BB - MAG_ALPHA_VV. If MAG_ALPHA_BB or MAG_ALPHA_VV is -99.99 the value for BBMINUSVV is also set to -99.99 .
- 68. W1MINUSVV: MAG_ALPHA_W1 - MAG_ALPHA_VV. If MAG_ALPHA_W1 or MAG_ALPHA_VV is -99.99 the value for W1MINUSVV is also set to -99.99 .
- 69. RED: $E(B - V)$ as found in Schlegel et al. (1998). Galactic extinction can be corrected using the procedure described in Cardelli et al. (1989). The extinction in the UVOT bands can be expressed as,

$$A_\lambda = E(B - V)[aR_v + b], \quad (2)$$

where $R_v = 3.1$ and λ is the UVOT filter (uvw2, uvm2, uvw1, *u*, *b*, and *v*). The values for *a* in each filter are -0.0581 , 0.0773 , 0.4346 , 0.9226 , 0.9994 , and 1.0015 , respectively. The values for *b* are 8.4402 , 9.1784 , 5.3286 , 2.1019 , 1.0171 , and 0.0126 , respectively. All values for *a* and *b* were determined as described in Cardelli et al. (1989). No correction factor is provided for the *white* filter as the large width of the FWHM makes any extinction correction highly dependent on the spectral energy distribution of the source.

70. NH: The logarithm of the absorption column density (N_H) along the line of sight as defined in Kalberla et al. (2005).

71. ZZ: The redshift of the burst. If no redshift was found the value is set to 99.9999.

72. ZZ_METH: The flag indicating how the redshift was determined. The flag is an integer from 0-4 representing: 0 = no redshift determined, 1 = absorption, 2 = emission, or 3 = Lyman break.

73. ZZ_GCN: The GCN Circular number where the information for ZZ and ZZ_METH was reported. If no redshift was reported this value is left blank.

74. FLUENCE_BAT: The prompt BAT fluence of the burst, in 10^{-8} erg cm $^{-2}$ (15 – 150 keV band), as reported in Sakamoto et al. (2007). If no fluence was reported, or for HETE2, INTEGRAL, or IPN discovered bursts, the value is set to -99.0 .

75. FLUX_RAD: The radio flux of the burst, in mJy, as reported in the GCN Circular. If an upper limit was reported the value is set to 99.000. If no radio observation was reported than the value is set to -99.000 .

76. FLUX_RAD_GCN: The GCN Circular number where the FLUX_RAD was reported. If no flux was reported this value is left blank.

77. RADIO_FREQ: The observed frequency of the detection in FLUX_RAD expressed in GHz.

78. DET_IR: Flag indicating whether a detection in the $R - K$ bands was reported in the GCN Circulars. “F” = No, “T” = Yes.

79. DET_UVOT: Flag indicating whether a detection in any of the UVOT bands was found. “F” = No, “T” = Yes.

80. DET_RADIO: Flag indicating whether a detection in the radio was reported in the GCN Circulars. “F” = No, “T” = Yes.

81. NOTES: Notes on individual objects.

5. Catalog Summary

From the catalog we can construct some of the general characteristics of the burst sample. Figure 5 displays the celestial coordinates of all UVOT observed GRBs, and whether or not they were detected. As is expected, the distribution of all bursts is random on the sky (cf. Meegan et al. 1992). From the sample of the 229 observed GRBs, $\sim 26\%$ are detected by

the UVOT at the 3σ -level (in an individual exposure), $\sim 60\%$ are detected by ground-based observations (although these are typically redder detections than reported by the UVOT) as reported in the GCNs, and $\sim 40\%$ have no reported detections.

The distribution of times to the start of the first observation (i.e. the settling exposure) by UVOT is shown in Figure 6. The median time to burst observation is 110 s for all observations. If only the main peak of the distribution is considered, i.e. the $\sim 70\%$ of the sample with $\Delta t < 300$ s, the median time to burst observation is 86 s. In most cases the UVOT is observing the very early stages of the afterglow. In some cases, UVOT is observing during the end of the prompt emission phase. The delay in observing the remaining $\sim 30\%$ of bursts is typically due to Earth occultations or to the inherent lag time for non-*Swift* burst alerts.

Figure 7 illustrates the distribution of exposure times in each filter in the first 2000 s following the GRB detection, as well as the total exposure in each filter for all bursts. Because the finding charts are typically taken in the *white* and *v* filters, and since the finding charts dominate the observing time during the first ~ 2000 s, the early light curves predominantly have *white* and *v* data points.

The distribution of the brightest UVOT *v*-filter magnitudes for each detected burst, which is almost always the first or second exposure, is shown in Figure 8. For time-to-observation of bursts < 500 s and for Galactic reddening < 0.5 the UVOT pipeline detects in a *single* exposure (i.e. no coadding of frames) an afterglow in $\sim 27\%$ of the cases. For time-to-observation of bursts ≥ 500 s and for Galactic reddening < 0.5 the UVOT pipeline detects in a *single* exposure an afterglow $\sim 22\%$ of the time. If these samples of early and late observed bursts are subdivided into long ($T_{90} > 2$ s) and short ($T_{90} \leq 2$ s) bursts, then the detection rate for a single exposure is $\sim 27\%$ for both long and short for the early observed bursts, while it is $\sim 29\%$ for the long and $\sim 12\%$ for the short late observed bursts. These values will increase as future versions of the catalog use optimal coaddition (see Section 6). Initial work indicates that for bursts observed within 500 s and for Galactic reddening < 0.5 the UVOT pipeline detects an afterglow in $\sim 40\%$ of the cases. Many of the remaining $\sim 60\%$ of “dark” bursts can be explained by circumburst extinction, high redshift Lyman- α blanketing and absorption, and suppression of the reverse shock (cf. Roming et al. 2006b; Fynbo et al. 2001; Groot et al. 1998; Halpern et al. 1998).

We have fit power law models to the light curves of bursts that are well-sampled in the UVOT observations. The definition of “well-sampled” here is that for a single band, an afterglow must be detected in at least two independent images taken between 300 s and 1×10^5 s after the burst. A total of 42 bursts are considered “well-sampled.”

Often the first few points on a light curve, up to several hundred seconds after a burst, are not consistent with a single power law fit that describes the rest of the light curve (i.e. GRBs 050730, 050820A, 060124, 060206, & 060614; cf. Oates et al. 2008). In those cases, the early points have been omitted from the power law fit. The remaining points were fit with a function consisting of a single power law and a constant offset. The constant was included to account for any remaining residual in the sky subtraction, or to account for possible host galaxy contribution to the flux. The best fit parameters were determined by minimizing the χ^2 value of the fit to the coincidence loss corrected linear count rates and their errors. The values of the fit parameters are given in the *Swift* UVOT Burst Catalog. Light curves and fits are shown in Figure 9, for the well-sampled bursts in the bands for which there is the largest number of detections of a given burst afterglow. In the case of GRB 060218, a power-law is not a satisfactory description of the light curve, so its light curve is shown without a fit. Figure 10 shows the light curves in all seven UVOT filters for GRB 061007. The lower right panel of Figure 10 shows all of the light curves for GRB 061007 scaled to match the v band light curve fit at 2000 s.

We note that the light curves have been plotted on a log-linear scale as opposed to the traditional log-log scale. This is done for diagnostic reasons in order to examine if the light curves approach zero. If the light curve approaches zero then there is no host galaxy contributing to the overall results. If the light curve is above zero then there is host galaxy contribution. If the light curve was below zero then a problem was identified and fixed.

Up to this point, we have only illustrated light curves on the basis of the image database. Figure 11 demonstrates the light curve for GRB 060607A as generated from a version of the event database. The event database provides the capability to probe the very early development of the afterglow. A discussion of the early afterglow features is presented elsewhere (Oates et al. 2008).

From the light curves a study of the interrelationship between bursts can be made. The majority of the well-sampled light curves are fit by a single power-law after several hundred seconds. Figure 12 illustrates the distribution of temporal slopes across all filters and bursts while Figure 13 shows the distribution of temporal slopes as a function of filter. The temporal slope ranges from -0.09 to -3 . The average temporal slope for the entire sample is $\alpha = 0.96$ (the dispersion about the mean, $\sigma = 0.48$) which is consistent with other published results (Kann et al. 2007). For the individual filters the average α is 1.30 ($\sigma = 0.43$), 1.31 ($\sigma = 0.41$), 0.96 ($\sigma = 0.33$), 0.86 ($\sigma = 0.38$), 1.05 ($\sigma = 0.42$), 1.00 ($\sigma = 0.63$), and 0.83 ($\sigma = 0.36$) for the *uvw2*, *uvm2*, *uvw1*, *u*, *b*, *v*, and *white* filters, respectively. A Kolmogorov-Smirnov (KS) test between the UV and optical data sets (excluding the *white* filter) indicates that the probability of the two data sets being different is 0.087.

By using the temporal slopes, we have calculated the magnitude of the light curves at 2000 s in each available UVOT band. The average v -band magnitude at 2000 s is 18.02 ($\sigma = 1.59$). Figure 14 reveals the color-color relationship between the $uvw1$, b , and v colors. Typical values for $b - v$ are ~ 0.5 with a small amount of scatter. On the other hand, values for $uvw1 - v$ are ~ 0 with a large degree of scatter.

Figures 15 & 16 provide a comparison of the X-ray flux at 11 hours ($F_{X,11}$) in the 0.3 – 10 keV band, and the prompt γ -ray fluence (S_γ) in the 15 – 150 keV band to the optical flux at 2000 s (f_{2000})⁹. Evident from the figures is a general trend of X-ray flux or γ -ray fluence to correspond to optical brightness. Using the Spearman rank correlation, the data are strongly correlated ($p = 8.8 \times 10^{-4}$) and marginally correlated ($p = 0.0184$) for $F_{X,11}$ and S_γ , respectively. An X-ray-to-optical correlation has been suggested previously (Roming et al. 2006b; Rol et al. 2005; Jakobsson et al. 2004; De Pasquale et al. 2003). We note that none of these values have been corrected for redshift. This is outside the scope of this paper and left for future work.

We also provide the redshift distribution of the burst sample (see Figure 17). The redshifts were not determined by the UVOT but rather by spectroscopic measurements with ground based instruments. From the distribution it can be seen that the UVOT is sampling bursts across the entire redshift range up to the UVOT redshift limit of $z \sim 5.1$.

6. Future Work

This catalog is useful for examining the relationship between optically detected and undetected bursts. Future versions of the database will incorporate various enhancements to the current version. Some of these enhancements include: using filter dependent region files, more fully automating quality checks, adding functionality to the FTOOLS `uvotsource`, and optimal coaddition of images.

For the current version of the database, composite region files were used. Future versions would use filter dependent (non-composite) region files for each burst. There are several cases where a dense population of sources in the v filter make for a complicated background region file, while the field is not at all complicated in the UV filters. A better background estimate can be determined if separate region files were used.

Future databases may be able to reclaim some exposures flagged as “poor quality” im-

⁹The X-ray fluxes are provided by the *Swift* XRT team and will be published in an upcoming paper (Burrows et al. 2008). The prompt γ -ray fluences are found in Sakamoto et al. (2007).

ages. Our method for finding images contaminated by charge trails or diffraction spikes is to sum all images in a given filter and observation sequence, visually inspect them, and manually flag contaminated images. This works well for small apertures, but future databases will require photometry for each object in a wide range of apertures, which would potentially require a different set of quality files for each aperture size. A better way to handle this problem would be to identify bright stars in each field and determine whether the spacecraft roll angle would align any of them in the CCD readout direction so as to affect a given aperture at the GRB location. This eliminates the need for manual checking of a large number of images. By automating the process only the individual images that are contaminated would be flagged, as opposed to flagging entire observation sequences of images. Future databases would also check the photometric stability using field stars for each image.

Several improvements to the UVOT tools used in generating the database have been proposed. Currently, `uvotsource` is not capable of performing sigma clipping of background pixels. Adding this functionality would improve the background computations. Since `uvotsource` uses a Gaussian model of the background, it has difficulty in estimating images with extremely low background counts as we often see in UV images. Adding a Poisson or Binomial background model would greatly improve our results in some cases.

In this database version, no coaddition of the individual images was attempted. Future work will include optimal coaddition of the data using the method proposed by Morgan et al. (2008). Using this method will identify more detections from this and future databases.

We gratefully acknowledge the contributions from members of the *Swift* team at the Pennsylvania State University (PSU), University College London/Mullard Space Science Laboratory (MSSL), NASA/Goddard Space Flight Center, and our subcontractors, who helped make this instrument possible. This work is sponsored at PSU by NASA contract NAS5-00136 and at MSSL by funding from the Science and Technology Facilities Council (STFC).

Swift(UVOT)

REFERENCES

- Arimmoto, M., et al. 2005, GRB Coordinates Network, Circular Service, 4550, 1
- Barthelmy, S. D., Butterworth, P., Cline, T. L., Gehrels, N., Fishman, G. J., Kouveliotou, C., & Meegan, C. A. 1995, *Ap&SS*, 231, 235

- Barthelmy, S. D., Butterworth, P., Cline, T. L., & Gehrels, N., 1998, in AIP Conf. Proc. 428, 4th Huntsville Symp. on Gamma-Ray Bursts, ed. C. A. Meegan, R. D. Preece, & T. M. Koshut (New York: AIP), 139
- Barthelmy, S. D., et al. 2005, Space Sci. Rev., 120, 143
- Blustin, A. J., et al. 2006, ApJ, 637, 901
- Burrows, D. N., et al. 2005, Space Sci. Rev., 120, 165
- Burrows, D. N., et al. 2008, ApJ, in prep
- Butler, N. R. 2007, AJ, 133, 1027
- Campana, S., et al. 2006, Nature, 442, 1008
- Cardelli, J. A., Clayton, G. C., & Mathis, J. S. 1989, ApJ, 345, 245
- De Pasquale, M., et al. 2003, ApJ, 592, 1018
- De Pasquale, M., et al. 2007, MNRAS, 377, 1638
- Fynbo, J. U., et al. 2001, A&A, 369, 373
- Gehrels, N., et al. 2004, ApJ, 611, 1005
- Goad, M., et al. 2007, A&A, 468, 103
- Goad, M., et al. 2007, A&A, 476, 1401
- Groot, P. J., et al. 1998, ApJ, 493, L27
- Grupe, D., et al. 2006, ApJ, 645, 464
- Halpern, J. P., Thorstensen, J. R., Helfand, D. J., & Costa, E. 1998, Nature, 393, 41
- Hurley, K., et al. 2005, ApJS, 156, 217
- Hurley, K., et al. 2005, GRB Coordinates Network, Circular Service, 4172, 1
- Jakobsson, P., et al. 2004, ApJ, 617, L21
- Jester, S., et al. 2005, AJ, 130, 873
- Kalberla, P. M. W., Burton, W. B., Hartmann, D., Arnal, E. M., Bajaja, E., Morras, R., & Pöppel, W. G. L. 2005, A&A, 440, 775

- Kann, D. A., et al. 2007, ApJ, submitted (arXiv:0712.2186)
- Kawai, N., et al. 2005, GRB Coordinates Network, Circular Service, 4359, 1
- Kuin, N. P. M., & Rosen, S. R. 2008, MNRAS, 383, 383
- Mason, K. O., et al. 2006, ApJ, 639, 311
- Meegan, C. A., Fishman, G. J., Wilson, R. B., Horack, J. M., Brock, M. N., Paciesas, W. S., Pendleton, G. N., & Kouveliotou, C. 1992, Nature, 355, 143
- Monet, D. G., et al. 2003, AJ, 125, 984
- Morgan, A. N., et al. 2008, ApJ, accepted
- Oates, S. R., et al. 2007, MNRAS, 380, 270
- Oates, S. R., et al. 2008, MNRAS, in prep
- Olive, J. -F., et al. 2005, GRB Coordinates Network, Circular Service, 4124, 1
- Perri, M., et al. 2007, A&A, 471, 83
- Poole, T. S., et al. 2008, MNRAS, 383, 627
- Ricker, G. R. 1997, in All-Sky X-Ray Observations in the Next Decade, ed. M. Matsuoka & N. Kawai (Japan: RIKEN), 366
- Rol, E., Wijers, R. A. M. J., Kouveliotou, C., Kaper, L., & Kaneko, Y. 2005, ApJ, 624, 868
- Roming, P. W. A., et al. 2005, Space Sci. Rev., 120, 95
- Roming, P. W. A., et al. 2006, ApJ, 651, 985
- Roming, P. W. A., et al. 2006, ApJ, 652, 1416
- Sakamoto, T., et al. 2005, GRB Coordinates Network, Circular Service, 3189, 1
- Sakamoto, T., et al. 2007, ApJS, 175, 179
- Schady, P., et al. 2007, MNRAS, 380, 1041
- Schlegel, D. J., Finkbeiner, D. P., & Davis, M. 1998, ApJ, 500, 525
- Still, M., et al. 2005, ApJ, 635, 1187
- York, D. G., et al. 2000, AJ, 120, 1579

Table 1. *Swift*/UVOT Filter Characteristics^a

Filter	λ_c (Å)	FWHM (Å)	m_z (mag)	f_λ (10^{-16} ergs cm $^{-2}$ s $^{-1}$ Å $^{-1}$)
uvw2	1928	657	17.35 ± 0.04	6.20 ± 0.10
uvm2	2246	493	16.82 ± 0.03	8.50 ± 0.06
uvw1	2600	693	17.49 ± 0.03	4.00 ± 0.10
<i>u</i>	3465	785	18.34 ± 0.02	1.63 ± 0.02
<i>b</i>	4392	975	19.11 ± 0.02	1.47 ± 0.01
<i>v</i>	5468	769	17.89 ± 0.01	2.61 ± 0.01
<i>white</i>	3850	2600	20.29 ± 0.04	0.37 ± 0.05

^a λ_c is the central wavelength, m_z is the zero point, and f_λ is the flux density conversion factor for the filters. All values are from Poole et al. (2008), except for λ_c and FWHM for the *white* filter, which are from Roming et al. (2005).

Table 2. UVOT Observed GRBs Not In the Databases

OBJECT	RA _{J2000}	DEC _{J2000}	ERROR (arcsec)	Comments
GRB050215A	348.382	49.322	240	<i>Swift</i> GRB
GRB050922A	271.154	−32.024	210	INTEGRAL GRB
GRB050925	303.476	34.332	120	Possible <i>Swift</i> SGR
GRB051114	226.266	60.156	90	Untriggered <i>Swift</i> GRB
GRB060102	328.834	−1.838	168	<i>Swift</i> GRB
GRB060114	195.277	−4.748	120	INTEGRAL GRB
GRB060130	229.224	−36.912	120	INTEGRAL GRB
GRB060728	16.646	−41.390	180	Possible <i>Swift</i> GRB
GRB061218	149.238	−35.221	240	Weak, short <i>Swift</i> GRB

Table 3. Selected Sample from the *Swift*/UVOT Image Mode Burst Database

OBJECT	TSTART	EXPOSURE (seconds)	FILTER	MAG	MAG_ERR	SNR
GRB050525	138672238.421	9.679	V	13.97	0.06	16.3
GRB050525	138672397.228	9.613	B	15.17	0.06	16.0
GRB050525	138677707.262	885.569	UVM2	17.75	0.06	17.9
GRB050525	138700740.978	190.932	U	19.28	0.17	6.4

Note. — Table 3 is published in its entirety in the electronic edition of the *Astrophysical Journal*. A portion is shown here for guidance regarding its form and content.

Table 4. Selected Sample from the *Swift*/UVOT Event Mode Burst Database

OBJECT	TSTART	EXPOSURE (seconds)	FILTER	MAG
GRB060607a	1.71350008.193	9.993	white	17.23
GRB060607a	1.71350018.193	10.000	white	17.06
GRB060607a	1.71350028.193	10.000	white	16.74
GRB060607a	1.71350038.193	10.000	white	16.38

Note. — Table 4 is published in its entirety in the electronic edition of the *Astrophysical Journal*. A portion is shown here for guidance regarding its form and content.

Table 5. Selected Sample from the *Swift*/UVOT Burst Catalog

OBJECT	RA_BEST	DEC_BEST	POS_ERR	DISC_BY	T90	TRIGTIME
GRB050730	212.071208	−3.771917	0.50	0	156.5	144446303.2
GRB050801	204.145833	−21.928055	0.50	0	19.4	144613682.1
GRB050802	219.274250	27.786840	0.50	0	19.0	144670082.1
GRB050803	350.657958	5.785833	1.40	0	87.9	144789240.3

Note. — Table 5 is published in its entirety in the electronic edition of the *Astrophysical Journal*. A portion is shown here for guidance regarding its form and content.

Table 6. *Swift*/UVOT Image Mode Burst Database Format

Column	Format	Description
1	A10	Object ID <i>GRByymmssX</i>
2	F10.6	Right ascension (J2000.0) in decimal degrees
3	F10.6	Declination (J2000.0) in decimal degrees
4	F6.2	Positional uncertainty in arcseconds
5	F11.1	Time of burst trigger in mission elapsed time (MET)
6	A23	Time of burst trigger in Universal time
7	F13.3	Time of middle of exposure in MET
8	F13.3	Time of start of exposure in MET
9	F13.3	Time of end of exposure in MET
10	F8.3	Total exposure time in seconds with all correction applied
11	F8.3	Total elapsed time in seconds
12	A5	UVOT filter
13	I1	Binning factor
14	F4.1	Source aperture radius in arcseconds
15	F7.2	Area of the source region (SR) in square arcseconds
16	F8.2	Area of the background region (BR) in square arcseconds
17	F5.3	Image plate scale in arcseconds per pixel
18	F9.2	Total number of counts in SR
19	F9.2	Error in the total number of counts in SR
20	F9.2	Total number of counts in BR
21	F9.2	Error in the total number of counts in BR
22	F9.2	Total number of counts in standard SR
23	F9.2	Error in the total number of counts in standard SR
24	E11.4	Count rate in SR in counts per second
25	E11.4	Error in the SR count rate
26	E11.4	Count rate in BR per square arcseconds
27	E11.4	Error in the BR count rate per square arcseconds
28	E11.4	Global background rate in counts per second per square arcsecond
29	E11.4	Area of global background region in square arcseconds
30	E11.4	Count rate in coincidence loss region (CLR)
31	E11.4	Error in the count rate of the CLR
32	F5.3	Coincidence loss correction factor (CLCF) for CLR

Table 6—Continued

Column	Format	Description
33	F5.3	Error in the CLR CLCF
34	F5.3	CLCF for BR
35	F5.3	Error in the BR CLCF
36	F9.2	Coincidence loss corrected (CLC) counts in SR
37	F9.2	Error in the SR CLC counts
38	F9.2	CLC counts in BR
39	F9.2	Error in the BR CLC counts
40	E11.4	CLC raw count rate in SR
41	E11.4	Error in the SR CLC raw count rate
42	E11.4	CLC background surface count rate in counts per second per square arcsecond
43	E11.4	Error in the CLC background surface count rate
44	E11.4	Coincidence corrected net count rate
45	E11.4	Error in the coincidence corrected net count rate
46	F5.3	Aperture correction between a 3'' to 5'' aperture
47	F5.3	Aperture factor used to compute the count rate error
48	E11.4	CLC count rate use to calculate flux and magnitude
49	E11.4	Error on the CLC count rate use to calculate flux and magnitude
50	F5.2	Magnitude/upper-limit of the source (99.00 for upper-limit)
51	F5.2	1 σ error in magnitude (9.90E+01 for upper-limits)
52	F6.1	Signal-to-noise ratio calculated from columns 41 & 43
53	F5.2	Magnitude of the background per square arcseconds
54	F5.2	1 σ error in background in magnitude per square arcseconds
55	F5.2	“N”-sigma limiting magnitude
56	F3.1	Chosen parameter for “N”
57	F5.2	Magnitude at which the count rate is one count per CCD frame
58	E10.3	Flux density in $\text{erg s}^{-1} \text{cm}^{-2} \text{\AA}^{-1}$
59	E10.3	1 σ error in flux density in $\text{erg s}^{-1} \text{cm}^{-2} \text{\AA}^{-1}$
60	E10.3	Flux density of the sky in $\text{erg s}^{-1} \text{cm}^{-2} \text{\AA}^{-1} \text{arcsec}^{-2}$
61	E10.3	1 σ error in sky flux density in $\text{erg s}^{-1} \text{cm}^{-2} \text{\AA}^{-1} \text{arcsec}^{-2}$
62	E10.3	“N”-sigma limiting flux density in $\text{erg s}^{-1} \text{cm}^{-2} \text{\AA}^{-1}$
63	E10.3	Flux density in $\text{erg s}^{-1} \text{cm}^{-2} \text{\AA}^{-1}$ at which the count rate is one count per frame

Table 6—Continued

Column	Format	Description
64	E10.3	Flux density in mJy
65	E10.3	1σ error in flux density in mJy
66	E10.3	Flux density of the sky in mJy arcsec ⁻²
67	E10.3	1σ error in sky flux density in mJy arcsec ⁻²
68	E10.3	“N”-sigma limiting flux density in mJy
69	E10.3	Flux density in mJy at which the count rate is one count per frame
70	F10.6	Right ascension (J2000.0) in decimal degrees of closest non-GRB source
71	F10.6	Declination (J2000.0) in decimal degrees of closest non-GRB source
72	F6.2	Magnitude in the given UVOT band of closest non-GRB source
73	F10.6	Centroided right ascension (J2000.0) in decimal degrees
74	F10.6	Centroided declination (J2000.0) in decimal degrees
75	F5.1	Centroided positional uncertainty in arcseconds
76	A1	Settling image flag (T/F)
77	A1	Aspect error flag (T/F)
78	A1	Charge trailing flag (T/F)
79	A1	Crowded field flag (T/F)
80	A1	Diffraction spike flag (T/F)
81	A1	Edge of field flag (T/F)
82	A1	In halo flag (T/F)
83	A1	Poor quality flag (T/F)
84	A8	Swift trigger number
85	A12	Name of source FITS extension
86	A54	Image name

Table 7. *Swift*/UVOT Event Mode Burst Database Format

Column	Format	Description
1	A10	Object ID <i>GRByymmssX</i>
2	F10.6	Right ascension (J2000.0) in decimal degrees
3	F10.6	Declination (J2000.0) in decimal degrees
4	F6.2	Positional uncertainty in arcseconds
5	F13.3	Time of burst trigger in MET
6	A23	Time of burst trigger in Universal time
7	F13.3	Time of middle of exposure in MET
8	F13.3	Time of start of exposure in MET
9	F13.3	Time of end of exposure in MET
10	F8.3	Total exposure time in seconds with all correction applied
11	F8.3	Total elapsed time in seconds
12	A5	UVOT filter
13	I1	Binning factor
14	F4.1	Source aperture radius in arcseconds
15	F7.2	Area of the SR in square arcseconds
16	F10.2	Area of the BR in square arcseconds
17	F5.3	Image plate scale in arcseconds per pixel
18	F6.3	CLCF for CLR
19	F5.3	Error in the CLR CLCF
20	F5.3	CLCF for BR
21	F5.3	Error in the BR CLCF
22	E11.4	CLC raw count rate in SR
23	E11.4	Error in the SR CLC raw count rate
24	E11.4	CLC background surface count rate in counts per second per square arcsecond
25	E11.4	Error in the CLC background surface count rate
26	E11.4	Coincidence corrected net count rate
27	E11.4	Error in the coincidence corrected net count rate
28	F5.3	Aperture correction between a 3'' to 5'' aperture
29	E11.4	CLC count rate use to calculate flux and magnitude
30	E11.4	Error on the CLC count rate use to calculate flux and magnitude
31	F5.2	Magnitude/upper-limit of the source (99.00 for upper-limit)
32	F5.2	1 σ error in magnitude (9.90E+01 for upper-limits)

Table 7—Continued

Column	Format	Description
33	E10.3	Flux density in $\text{erg s}^{-1} \text{cm}^{-2} \text{\AA}^{-1}$
34	E10.3	1σ error in flux density in $\text{erg s}^{-1} \text{cm}^{-2} \text{\AA}^{-1}$
35	F10.6	Centroided right ascension (J2000.0) in decimal degrees
36	F10.6	Centroided declination (J2000.0) in decimal degrees
37	F5.1	Centroided positional uncertainty in arcseconds
38	A1	Settling image flag (T/F)
39	A1	Aspect error flag (T/F)
40	A8	Swift trigger number
41	A54	Event list filename

Table 8. *Swift*/UVOT Burst Catalog Format

Column	Format	Description
1	A10	Object ID <i>GRByymmssX</i>
2	F10.6	Right ascension (J2000.0) in decimal degrees
3	F10.6	Declination (J2000.0) in decimal degrees
4	F6.2	Positional uncertainty in arcseconds
5	A8	Reference for the given position and error
6	I1	Discovery flag
7	F5.1	T_{90} in seconds
8	F11.1	Time of burst trigger in mission elapsed time (MET)
9	A23	Time of burst trigger in Universal time
10	E13.6	Start time in seconds of 1st UVOT observation
11	F6.2	First reported magnitude (FRM) in the uvw2-filter
12	E13.6	Time since burst, in seconds, for the FRM in the uvw2-filter
13	F6.2	FRM in the uvm2-filter
14	E13.6	Time since burst, in seconds, for the FRM in the uvm2-filter
15	F6.2	FRM in the uvw1-filter
16	E13.6	Time since burst, in seconds, for the FRM in the uvw1-filter
17	F6.2	FRM in the <i>u</i> -filter
18	E13.6	Time since burst, in seconds, for the FRM in the <i>u</i> -filter
19	F6.2	FRM in the <i>b</i> -filter
20	E13.6	Time since burst, in seconds, for the FRM in the <i>b</i> -filter
21	F6.2	FRM in the <i>v</i> -filter
22	E13.6	Time since burst, in seconds, for the FRM in the <i>v</i> -filter
23	F6.2	FRM in the <i>white</i> -filter
24	E13.6	Time since burst, in seconds, for the FRM in the <i>white</i> -filter
25	F6.2	Peak reported magnitude (PRM) in the uvw2-filter
26	E13.6	Time since burst, in seconds, for the PRM in the uvw2-filter
27	F6.2	PRM in the uvm2-filter
28	E13.6	Time since burst, in seconds, for the PRM in the uvm2-filter
29	F6.2	PRM in the uvw1-filter
30	E13.6	Time since burst, in seconds, for the PRM in the uvw1-filter
31	F6.2	PRM in the <i>u</i> -filter
32	E13.6	Time since burst, in seconds, for the PRM in the <i>u</i> -filter
33	F6.2	PRM in the <i>b</i> -filter

Table 8—Continued

Column	Format	Description
34	E13.6	Time since burst, in seconds, for the PRM in the <i>b</i> -filter
35	F6.2	PRM in the <i>v</i> -filter
36	E13.6	Time since burst, in seconds, for the PRM in the <i>v</i> -filter
37	F6.2	PRM in the <i>white</i> -filter
38	E13.6	Time since burst, in seconds, for the PRM in the <i>white</i> -filter
39	F6.2	Temporal slope in the uvw2-filter
40	F6.2	Error in the temporal slope of the uvw2-filter
41	E9.2	Amplitude in the temporal slope of the uvw2-filter
42	F6.2	Magnitude in the uvw2-filter at 2000 s
43	F6.2	Temporal slope in the uvm2-filter
44	F6.2	Error in the temporal slope of the uvm2-filter
45	E9.2	Amplitude in the temporal slope of the uvm2-filter
46	F6.2	Magnitude in the uvm2-filter at 2000 s
47	F6.2	Temporal slope in the uvw1-filter
48	F6.2	Error in the temporal slope of the uvw1-filter
49	E9.2	Amplitude in the temporal slope of the uvw1-filter
50	F6.2	Magnitude in the uvw1-filter at 2000 s
51	F6.2	Temporal slope in the <i>u</i> -filter
52	F6.2	Error in the temporal slope of the <i>u</i> -filter
53	E9.2	Amplitude in the temporal slope of the <i>u</i> -filter
54	F6.2	Magnitude in the <i>u</i> -filter at 2000 s
55	F6.2	Temporal slope in the <i>b</i> -filter
56	F6.2	Error in the temporal slope of the <i>b</i> -filter
57	E9.2	Amplitude in the temporal slope of the <i>b</i> -filter
58	F6.2	Magnitude in the <i>b</i> -filter at 2000 s
59	F6.2	Temporal slope in the <i>v</i> -filter
60	F6.2	Error in the temporal slope of the <i>v</i> -filter
61	E9.2	Amplitude in the temporal slope of the <i>v</i> -filter
62	F6.2	Magnitude in the <i>v</i> -filter at 2000 s
63	F6.2	Temporal slope in the <i>white</i> -filter
64	F6.2	Error in the temporal slope of the <i>white</i> -filter
65	E9.2	Amplitude in the temporal slope of the <i>white</i> -filter
66	F6.2	Magnitude in the <i>white</i> -filter at 2000 s

Table 8—Continued

Column	Format	Description
67	F6.2	$b - v$ at 2000 s
68	F6.2	uvw1 $- v$ at 2000 s
69	F5.3	Galactic reddening
70	E8.2	Logarithm of Galactic HI column density ($\log N_H$)
71	F7.4	Redshift
72	I1	Redshift type flag
73	I4	GCN Circular number where redshift was reported
74	E9.2	Prompt BAT fluence in erg cm^{-2} as reported by Sakamoto et al. (2007)
75	F7.3	Radio flux in mJy as reported in GCN
76	I4	GCN Circular number where radio flux was reported
77	F6.2	Frequency in GHz of radio detection as reported in GCN
78	A1	Flag indicating a detection in the $R - K$ band was reported in GCN Circulars
79	A1	Flag indicating a detection in a UVOT band
80	A1	Flag indicating a detection in the radio was reported in GCN Circulars
81	A256	Notes

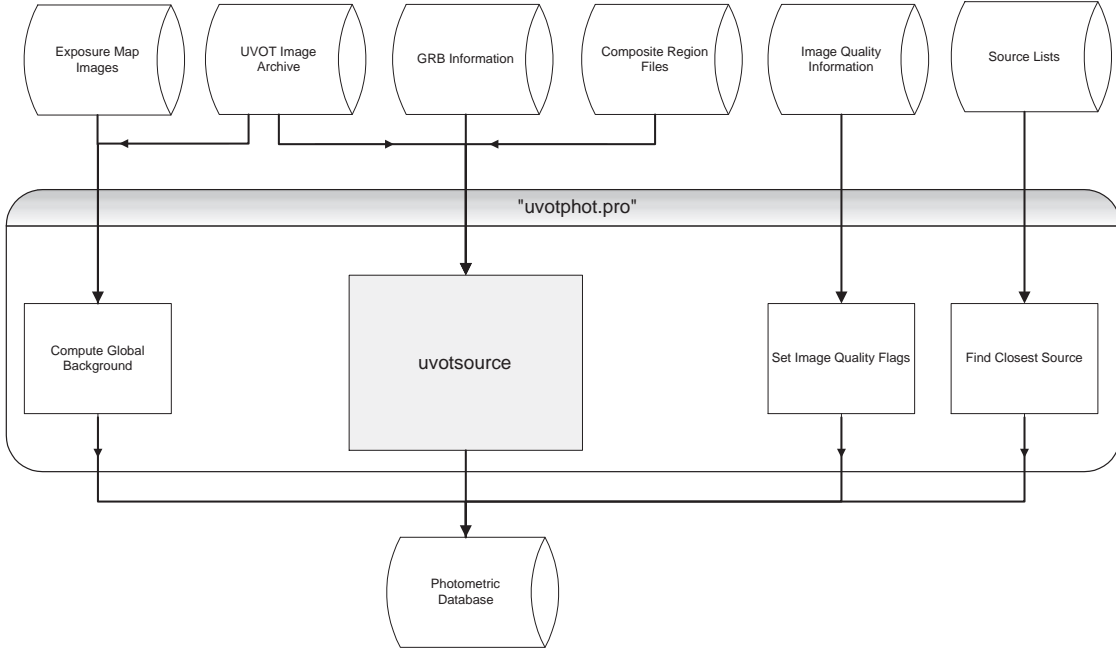


Fig. 1.— Flowchart of the photometric pipeline software used to create the database.

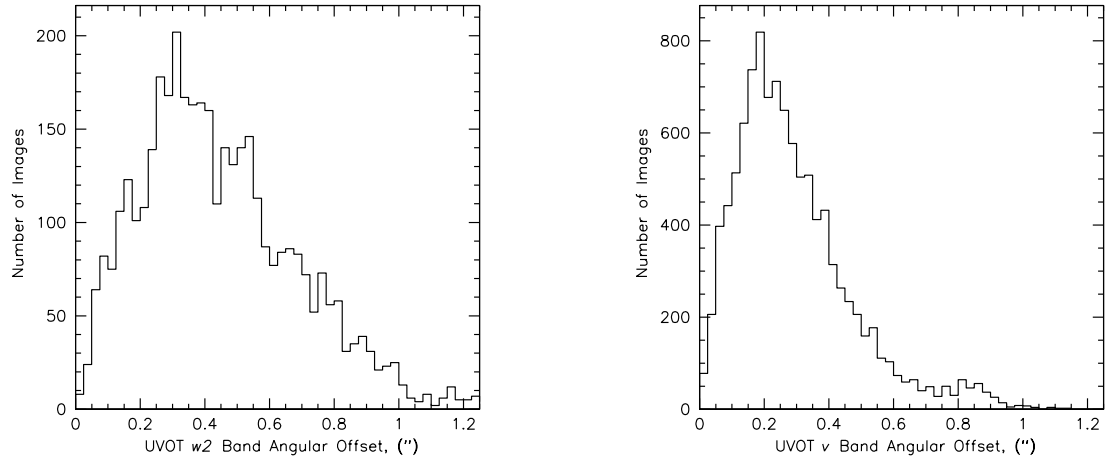


Fig. 2.— Distribution of angular offsets with respect to the USNO-B1 catalog for field stars observed with the uvw2 (*left*) and *v* (*right*) filters. The absolute accuracy is $0''.31$ and $0''.19$ for the uvw2 and *v* filters, respectively. The internal astrometric precision is $0''.27$ and $0''.21$ for the uvw2 and *v* bands respectively.

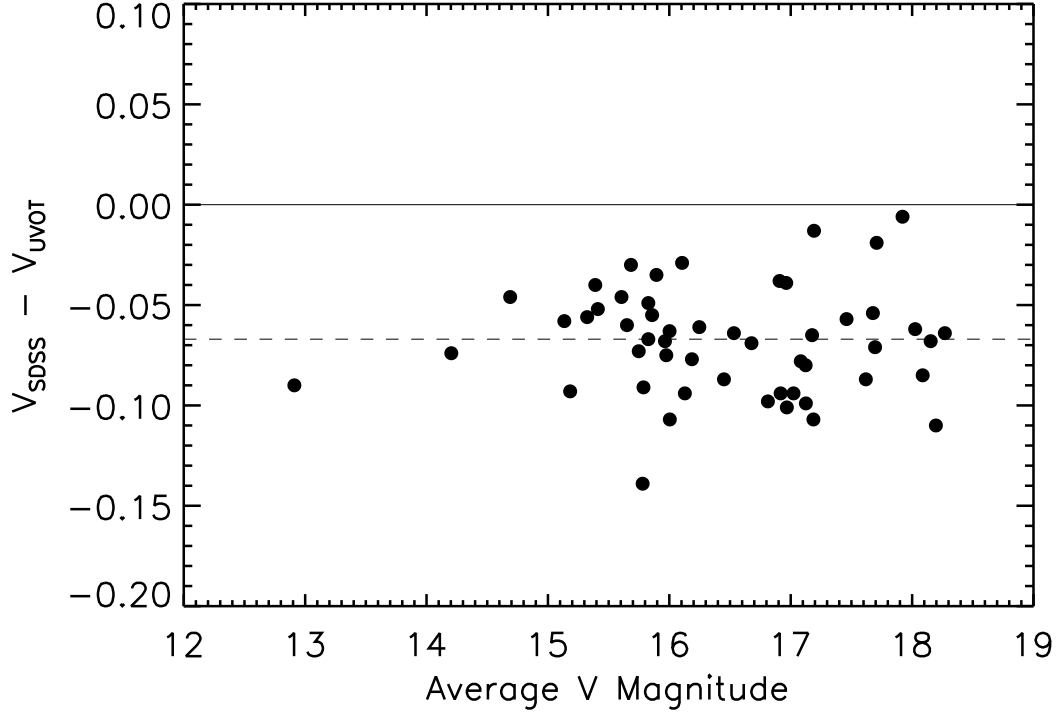


Fig. 3.— The absolute photometric accuracy for the v filter. Comparing stars from the SDSS database with UVOT observations and adjusting to the Johnson V magnitude produces a median absolute photometric offset (dotted line) between the SDSS and UVOT for the v filter of -0.068 magnitudes (3σ confidence limit).

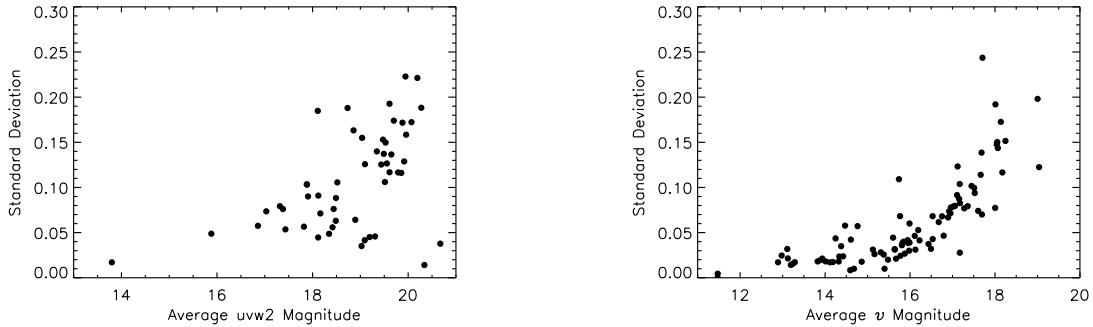


Fig. 4.— Internal photometric precision for the uvw2 (*left*) and v (*right*) filter data sets for exposure times greater than 90 s.

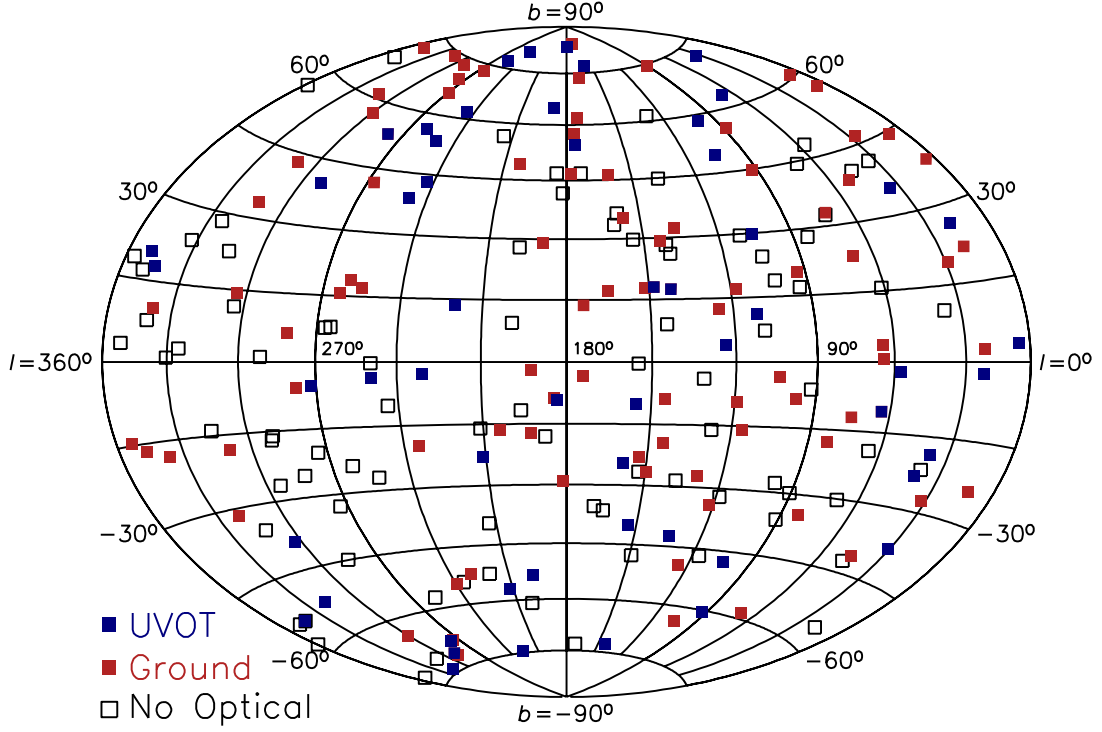


Fig. 5.— Coordinates on a Galactic Aitoff projection of 229 UVOT observed GRBs in the first ~ 2.5 years. Open squares are undetected afterglows by UVOT or ground-based telescopes, blue squares are afterglows detected by UVOT, and red squares are afterglows detected by ground based telescopes. [*See the electronic edition of the Journal for a color version of this figure.*]

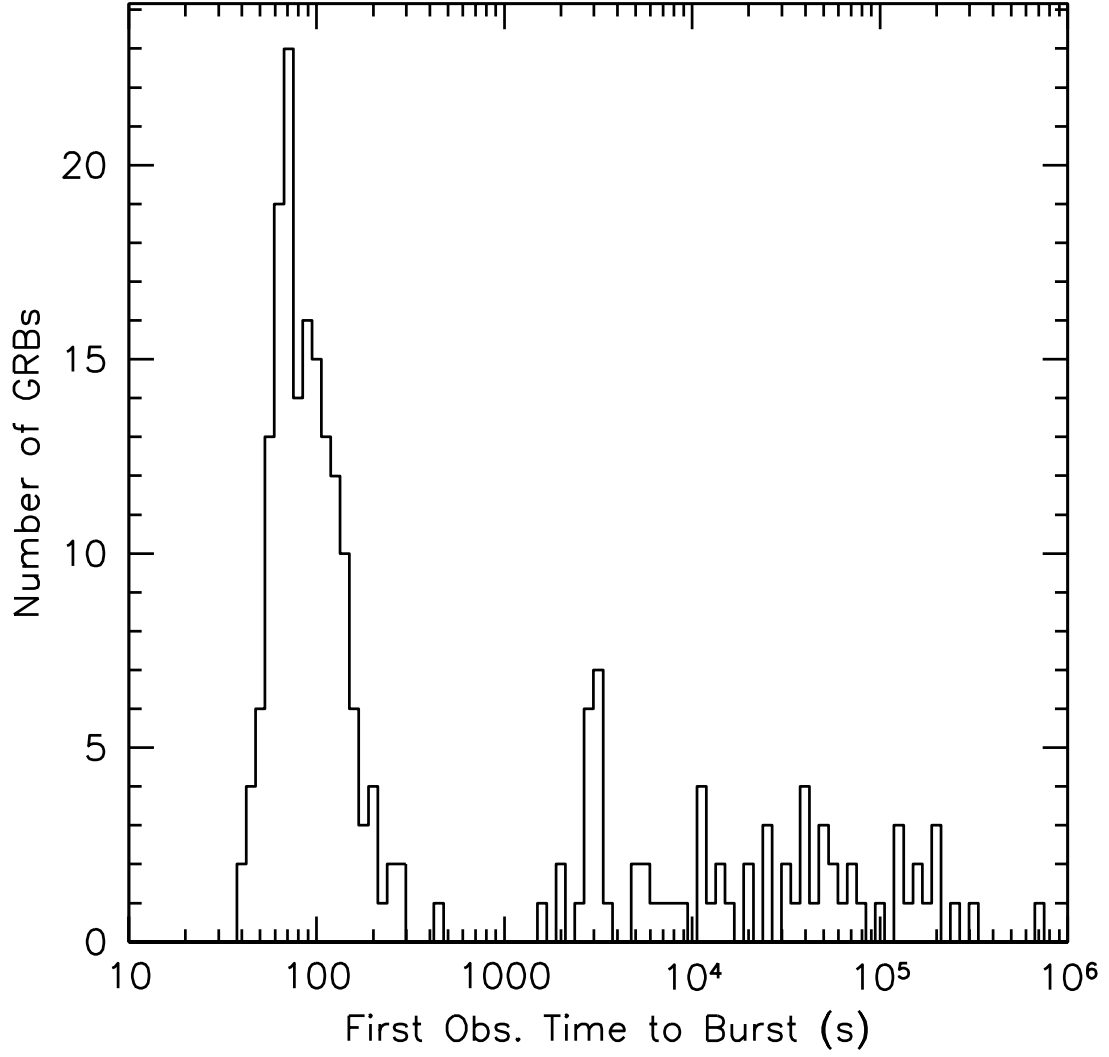


Fig. 6.— The distribution of times for the first observation of a GRB, including settling exposures. The median time to burst observations is 110 s for all observations. The median time to burst observations is 86 s if only the main peak is considered.

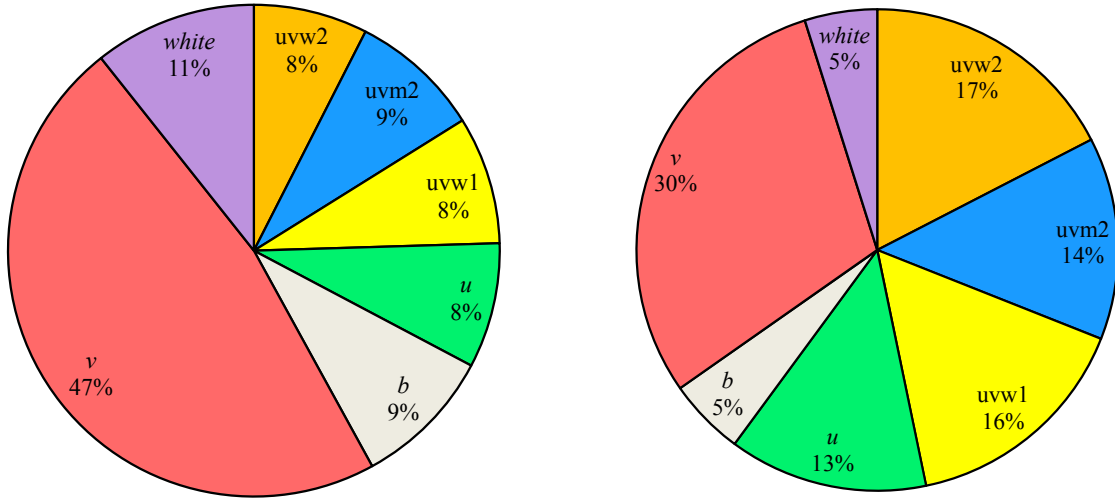


Fig. 7.— The distribution of time spent in each filter in observing all bursts in the first 2000 s (*left*) following the burst detection and for the cumulative time (*right*) for all bursts. [See the electronic edition of the *Journal* for a color version of this figure.]

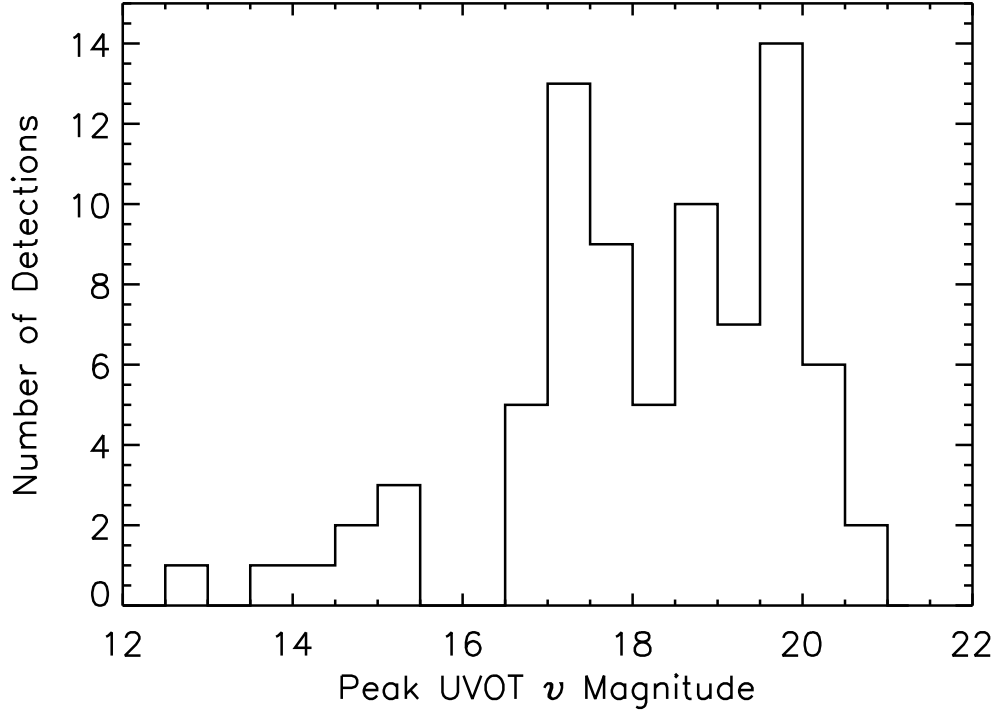


Fig. 8.— Distribution of the brightest UVOT v -filter magnitudes for each detected burst for a total of 79 points in the histogram. For time-to-observation of bursts < 500 s and for galactic reddening < 0.5 , the UVOT pipeline detects in a *single* exposure (no coadding of data) an afterglow in $\sim 27\%$ of the cases. For time-to-observation of bursts ≥ 500 s and for Galactic reddening < 0.5 , the UVOT pipeline detects in a *single* exposure an afterglow $\sim 22\%$ of the time.

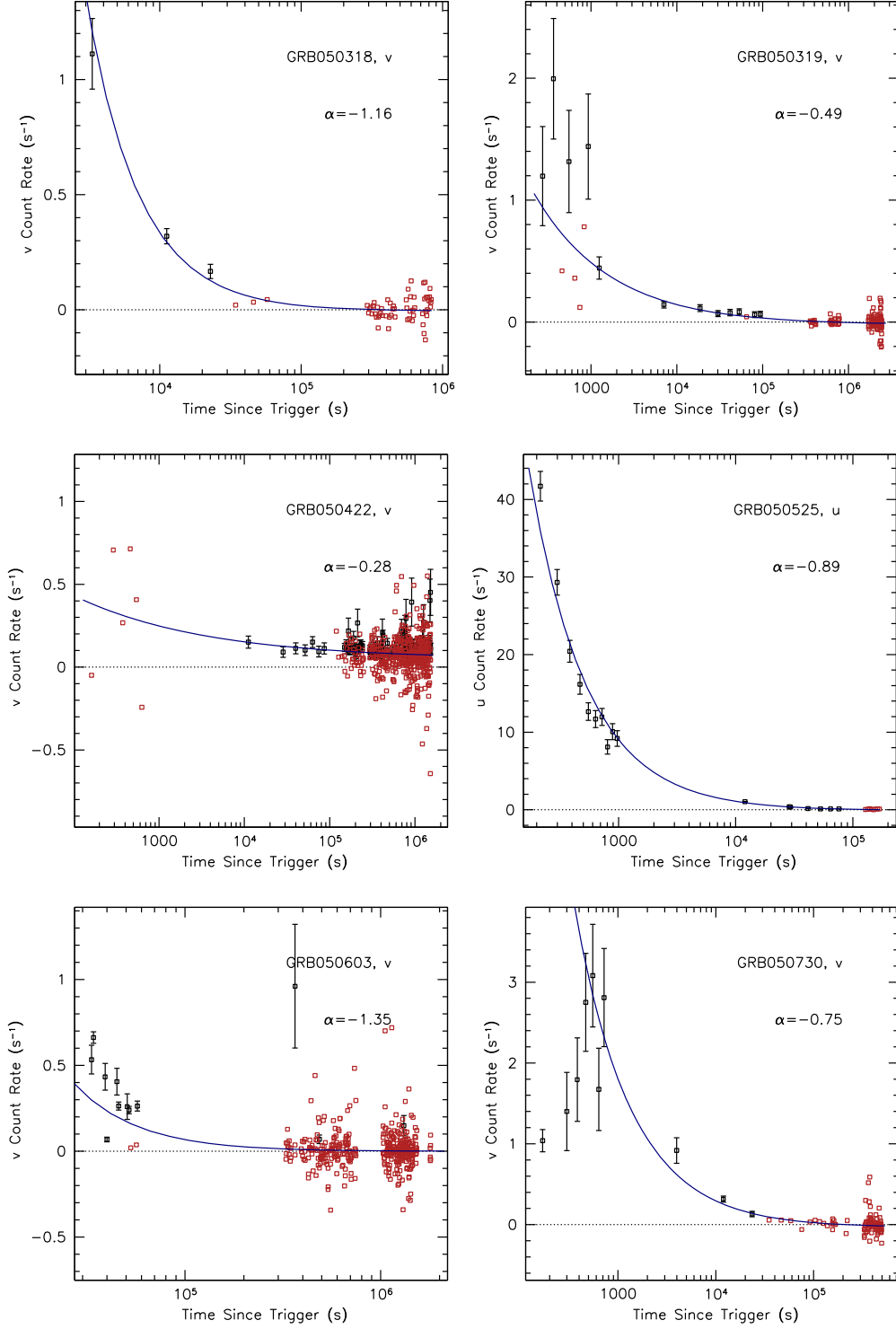


Fig. 9a.— Light curves of all “well” sampled bursts in one UVOT band (part 1 of 7). The name of the burst, the UVOT band displayed, and the temporal slope are provided. Black points are UVOT detections and red points are upper limits. [*See the electronic edition of the Journal for a color version of this figure.*]

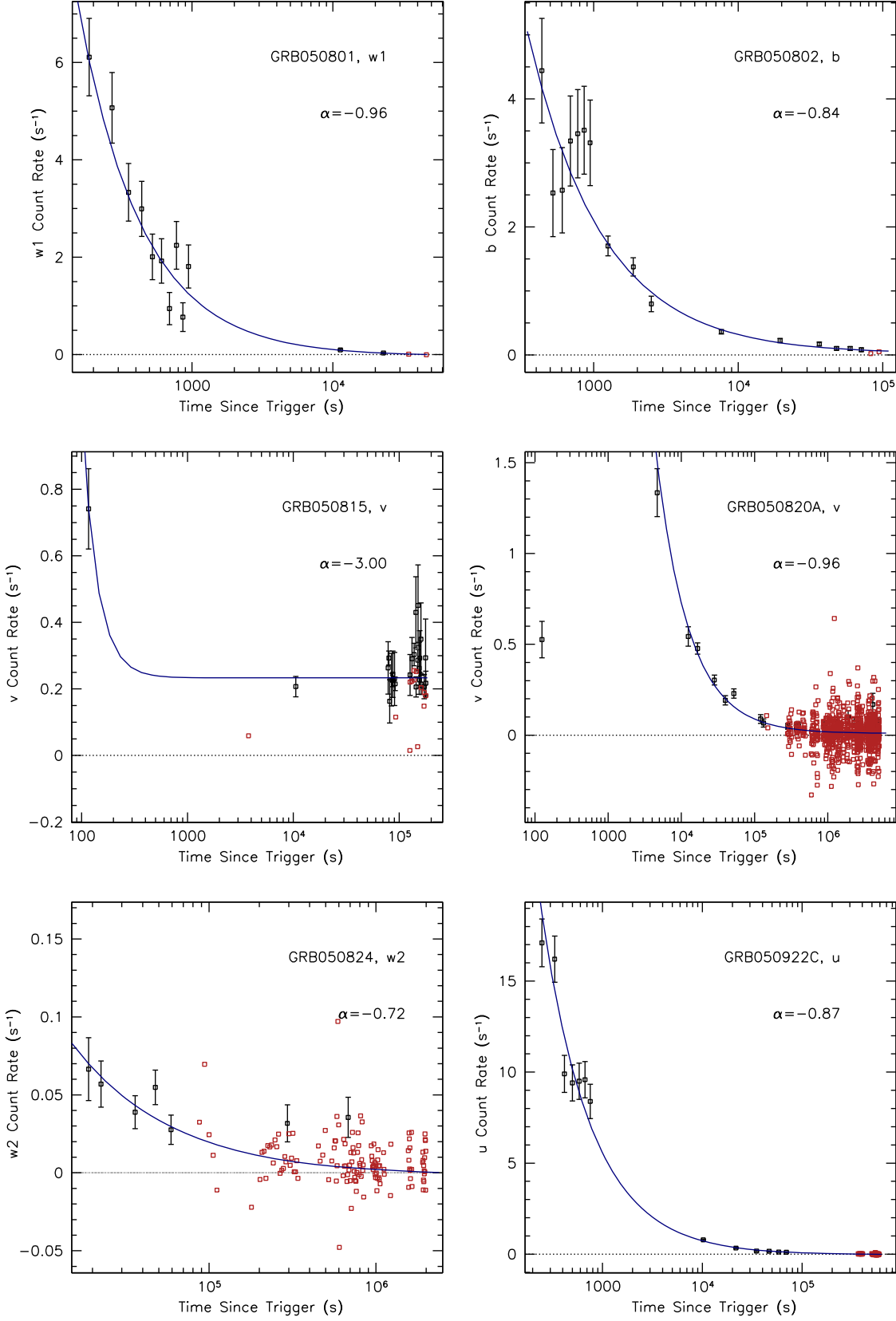


Fig. 9b.— Light curves of all “well” sampled bursts in one UVOT band (part 2 of 7).

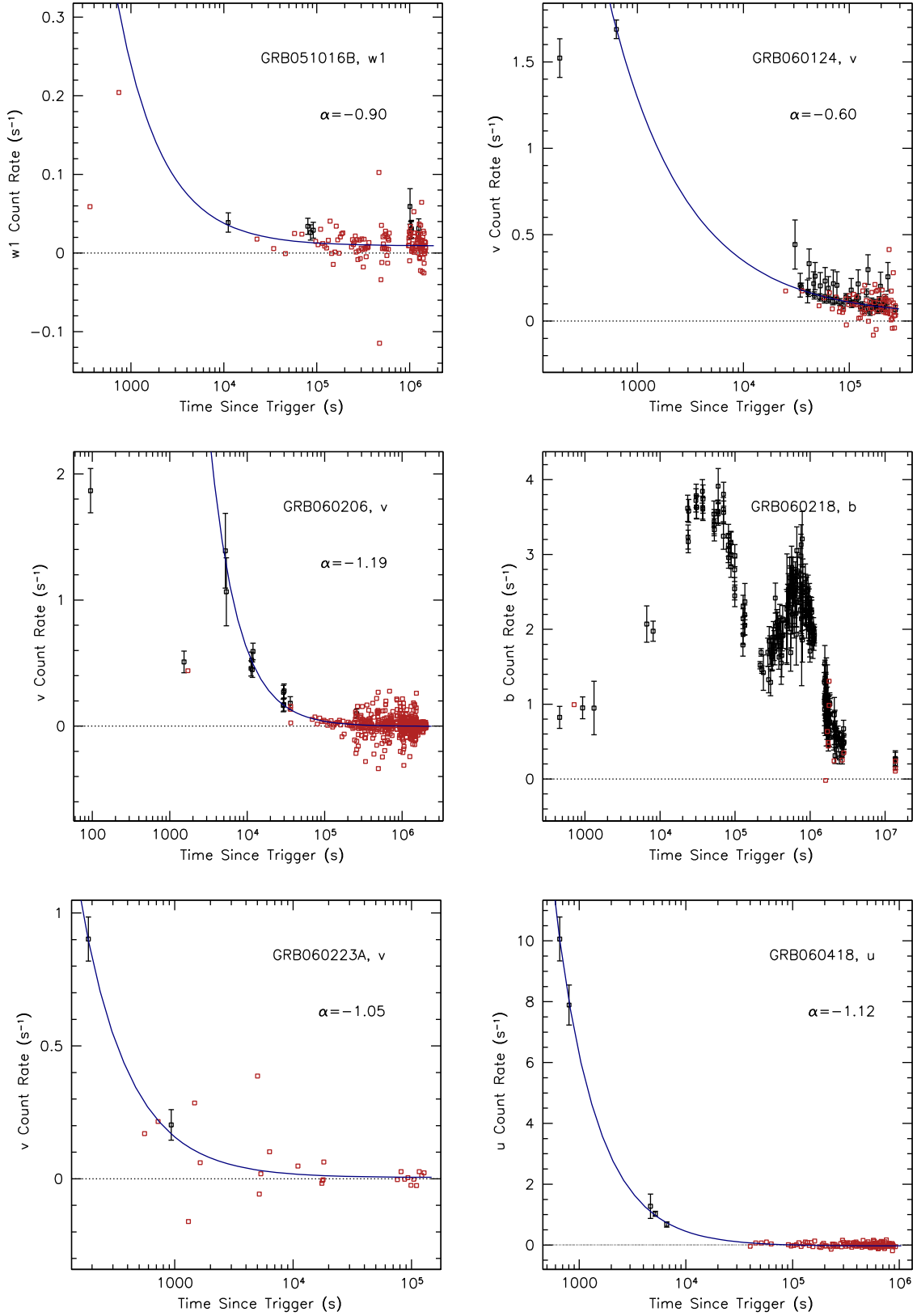


Fig. 9c.— Light curves of all “well” sampled bursts in one UVOT band (part 3 of 7).

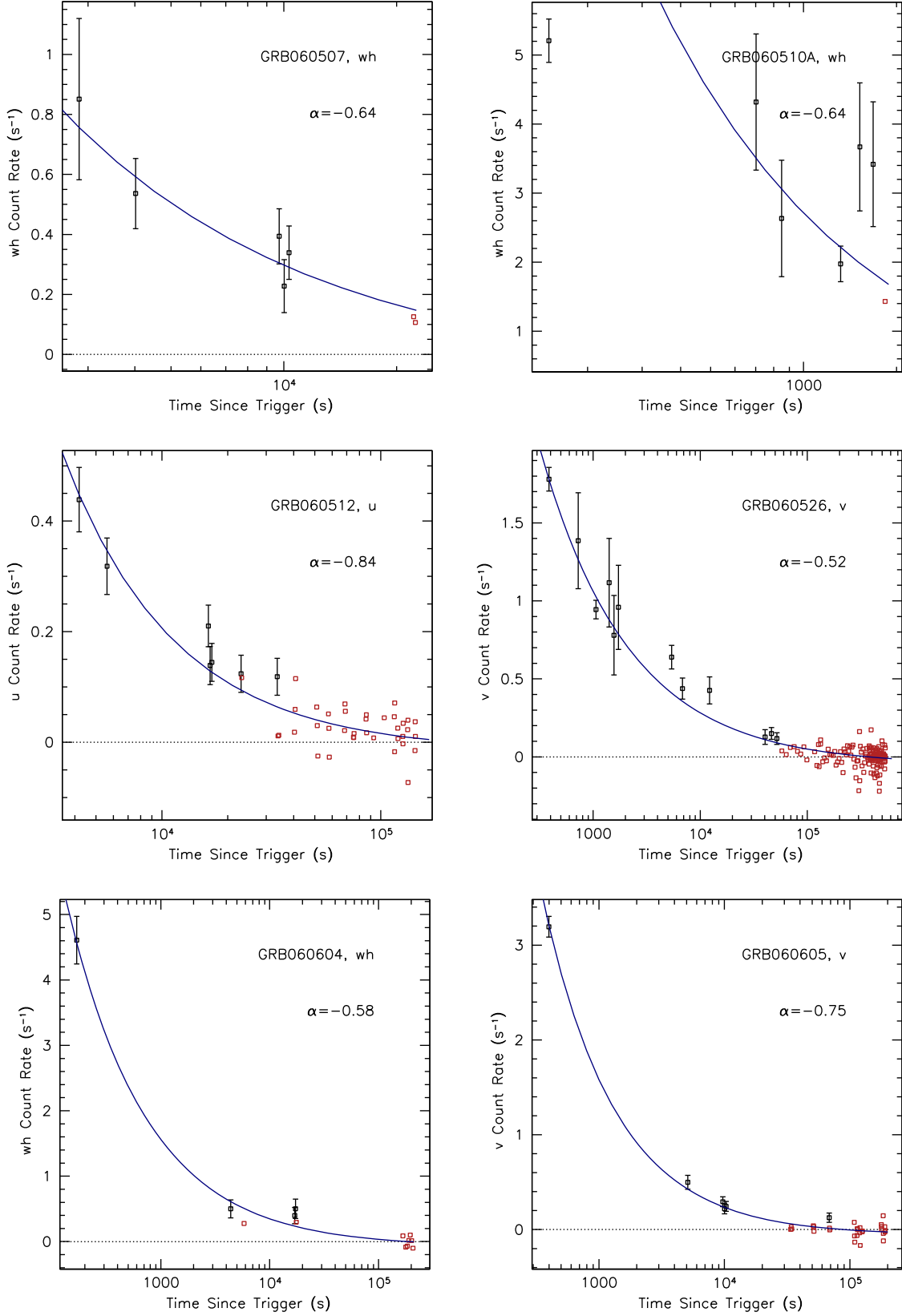


Fig. 9d.— Light curves of all “well” sampled bursts in one UVOT band (part 4 of 7).

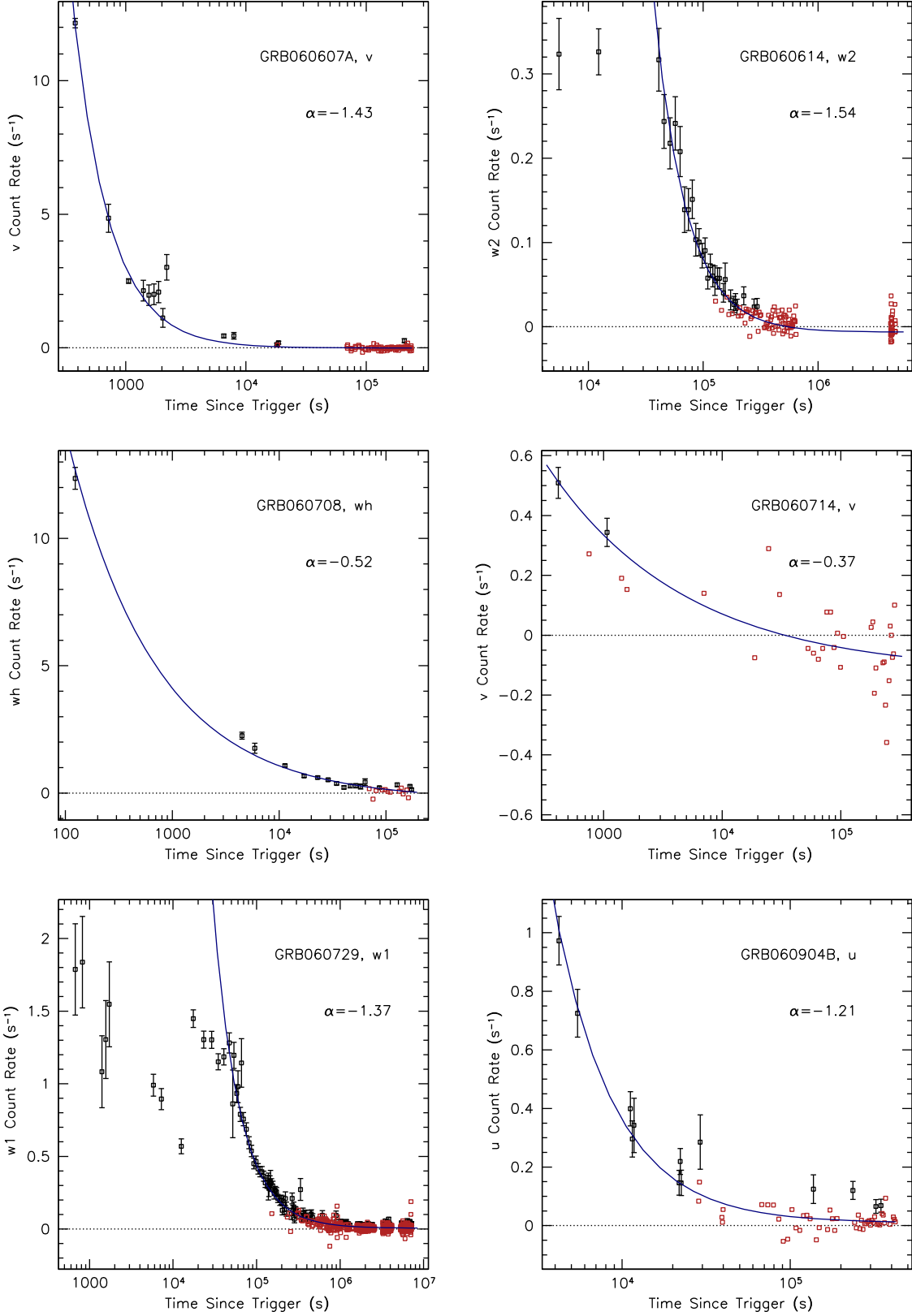


Fig. 9e.— Light curves of all “well” sampled bursts in one UVOT band (part 5 of 7).

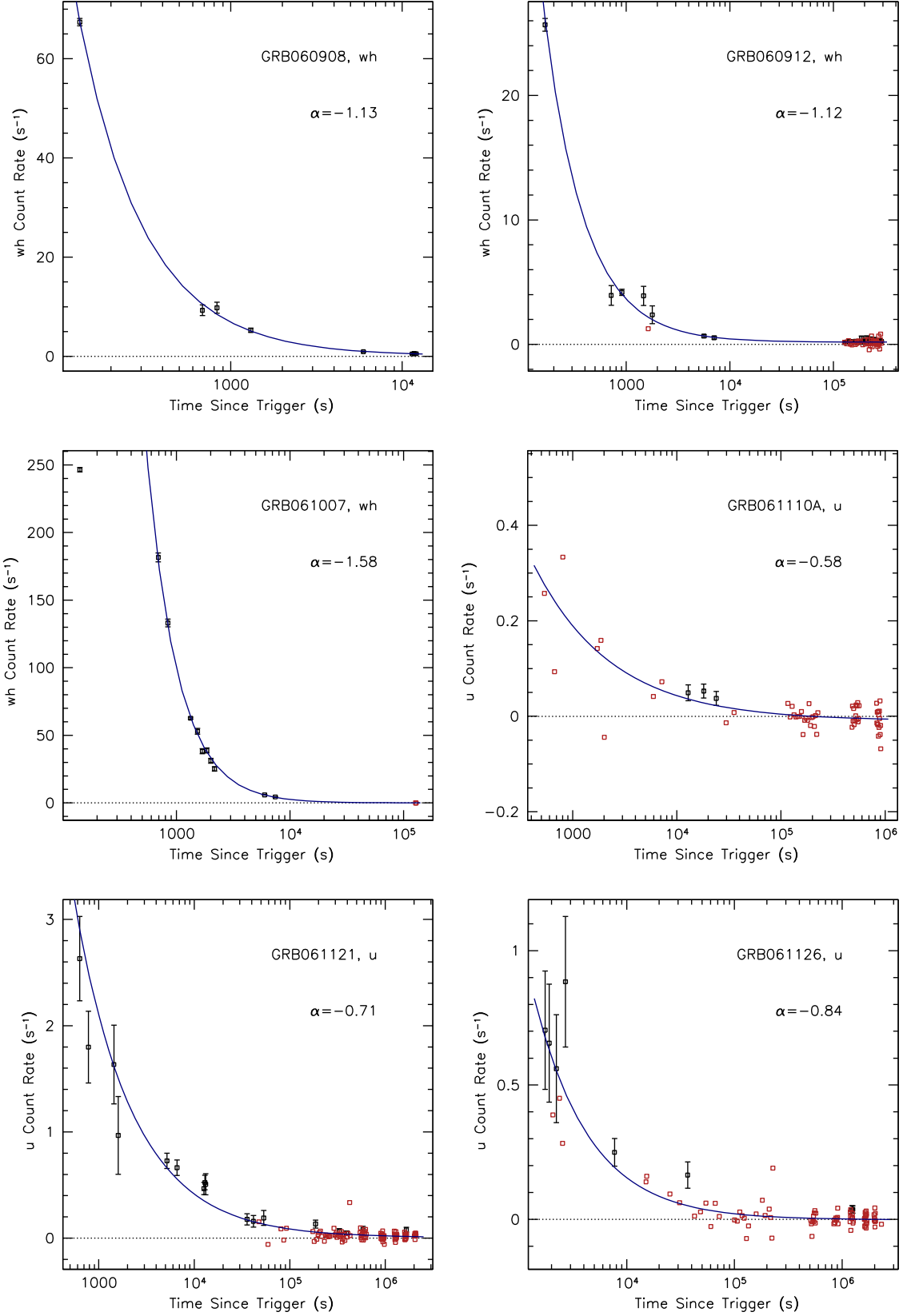


Fig. 9f.— Light curves of all “well” sampled bursts in one UVOT band (part 6 of 7).

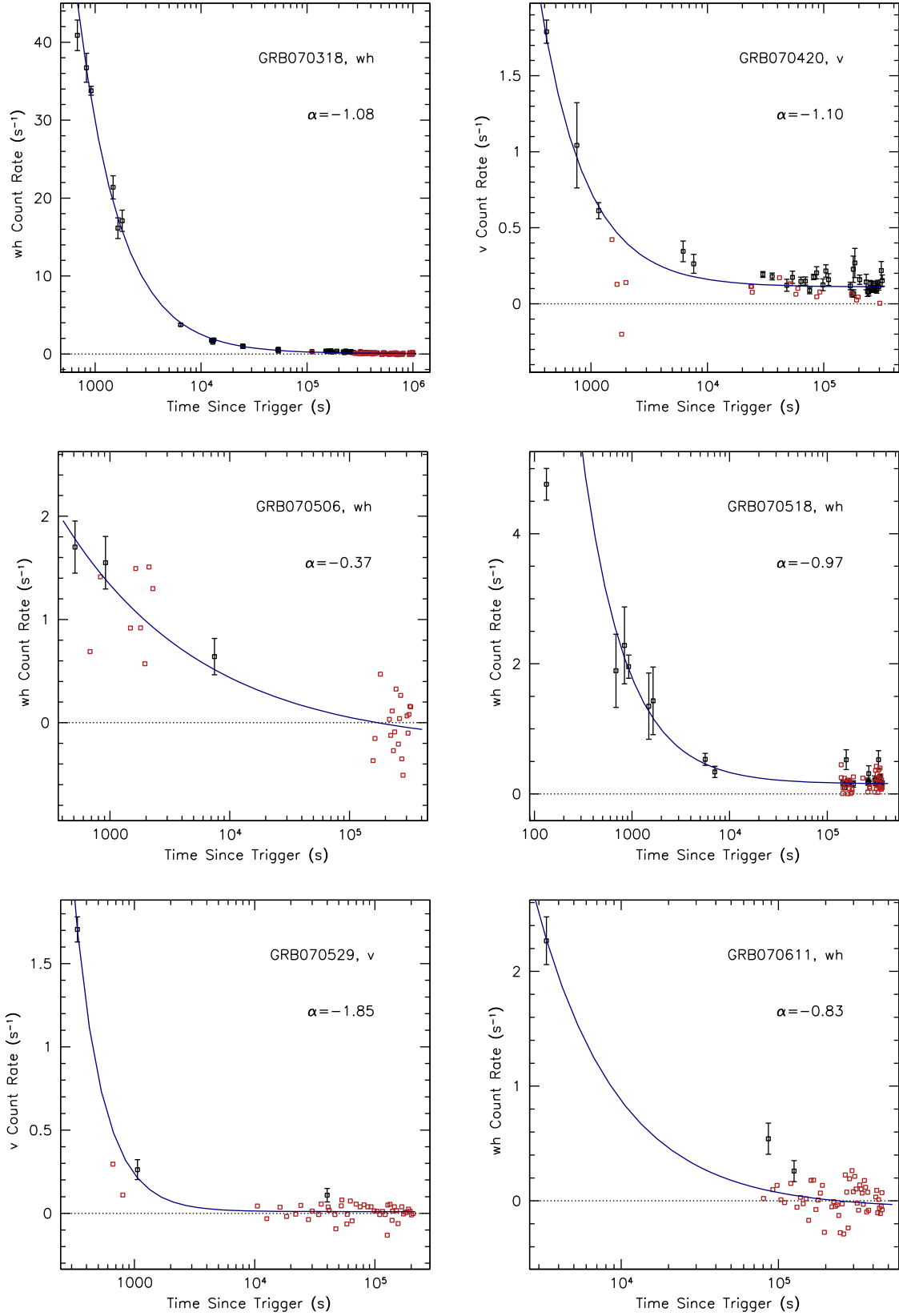


Fig. 9g.— Light curves of all “well” sampled bursts in one UVOT band (part 7 of 7).

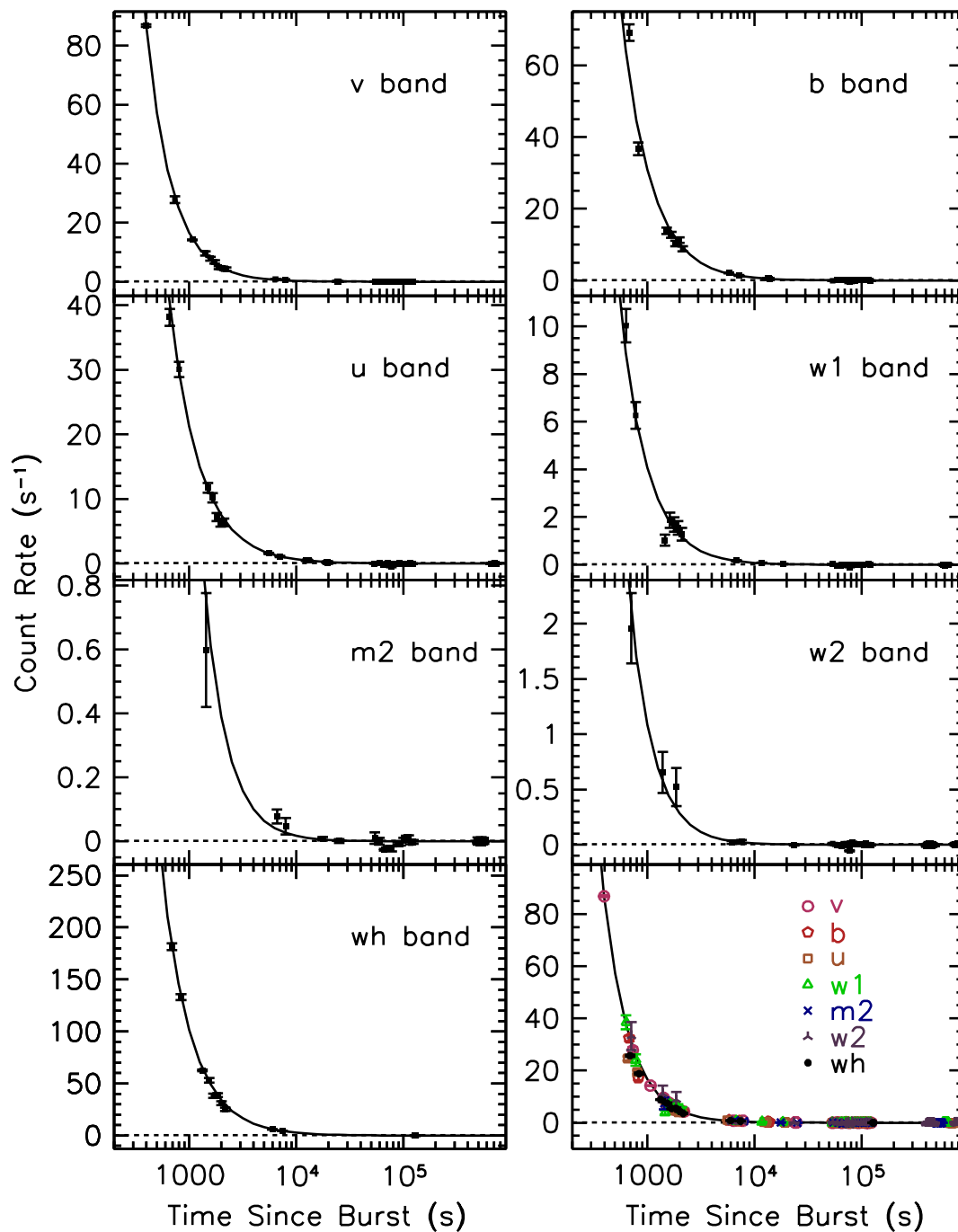


Fig. 10.— Light curves in each UVOT band for GRB 061007. [See the electronic edition of the Journal for a color version of this figure.]

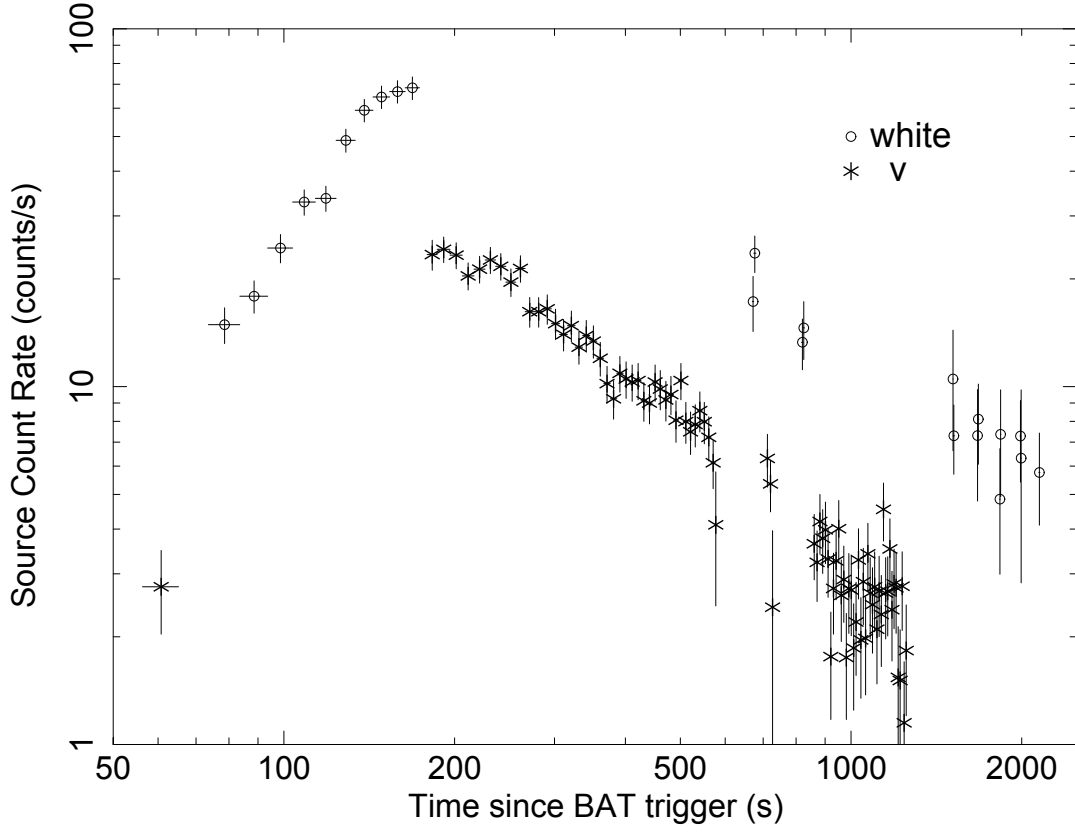


Fig. 11.— Light curve for GRB 060607A produced from a version of the event database. Typically, the taking of data in event mode has ceased by ~ 2000 s. The count rate is in counts s^{-1} . The v -band data point at ~ 62 s is produced while the spacecraft is settling on the target. The UVOT detector voltage is still changing during this period, therefore, the count rate is not calibrated for this situation.

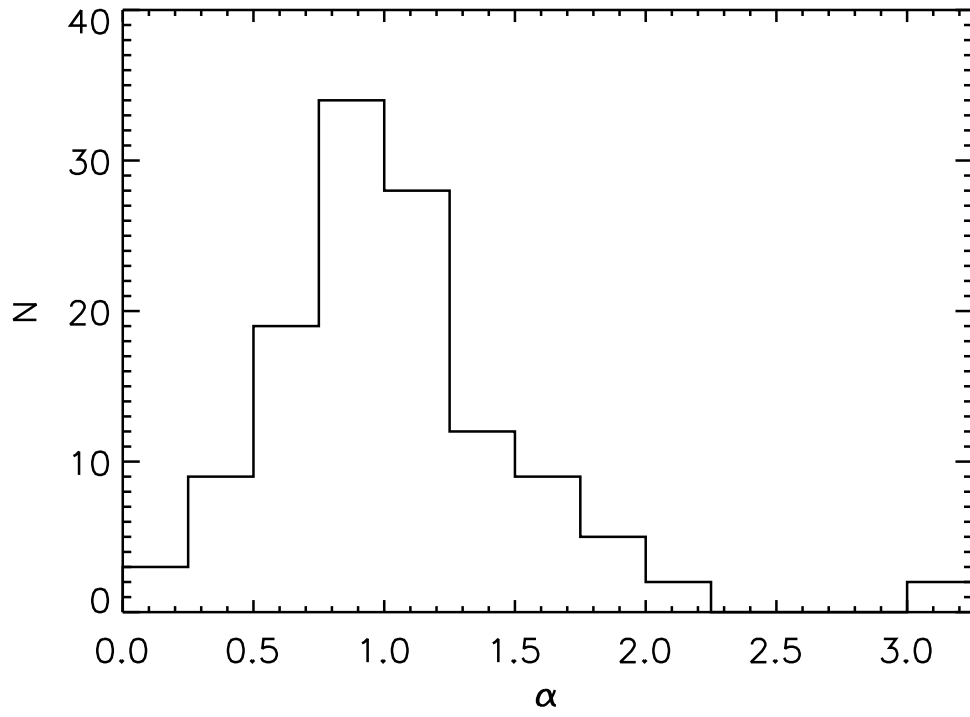


Fig. 12.— The filter independent temporal slope distribution for the 42 “well” sampled GRBs. The median temporal slope is $\alpha = 0.96$ ($\sigma = 0.48$).

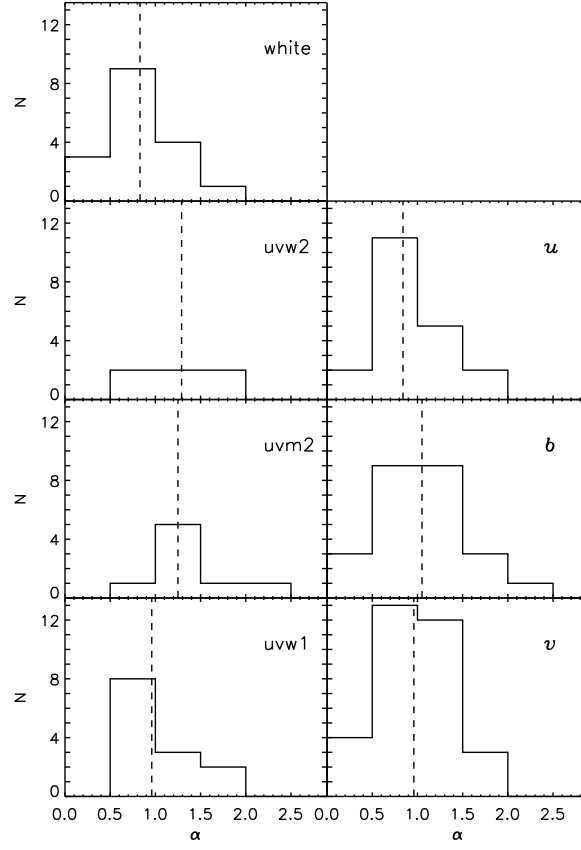


Fig. 13.— Temporal slope distribution in different UVOT filters. The median temporal slope is 1.30 ($\sigma = 0.43$), 1.31 ($\sigma = 0.41$), 0.96 ($\sigma = 0.33$), 0.86 ($\sigma = 0.38$), 1.05 ($\sigma = 0.42$), 1.00 ($\sigma = 0.63$), and 0.83 ($\sigma = 0.36$) for the *uvw2*, *uvm2*, *uvw1*, *u*, *b*, *v*, and *white* filters, respectively.

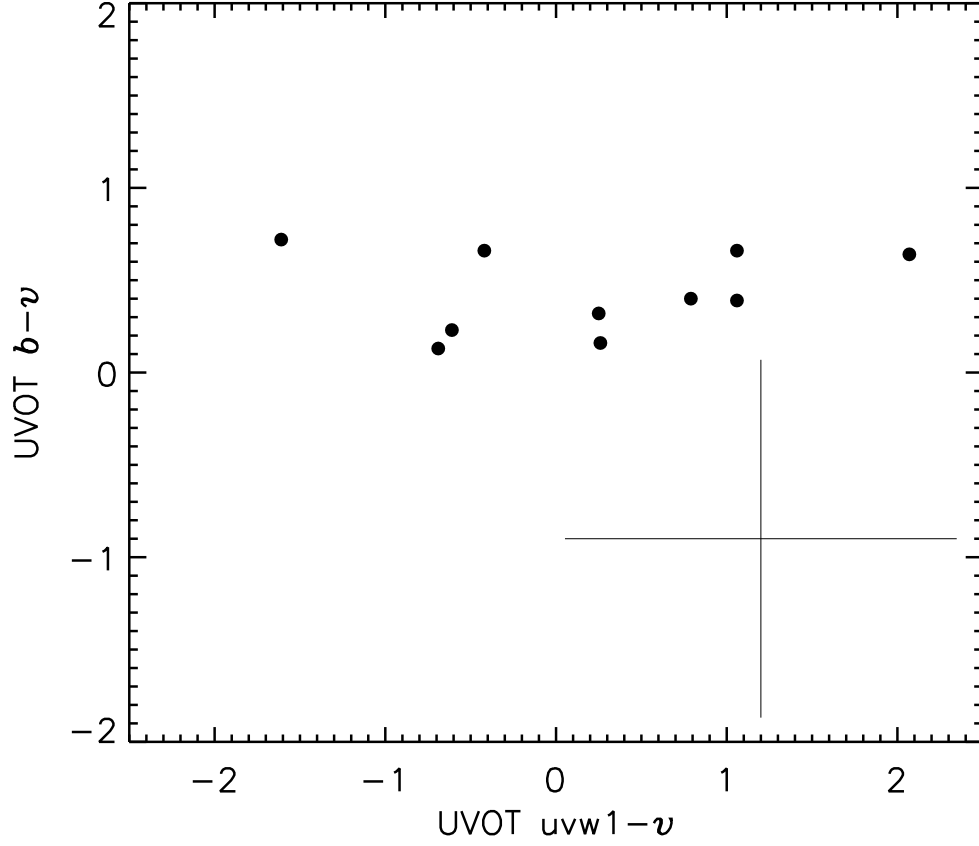


Fig. 14.— Distribution of afterglow colors as measured by the UVOT for bursts in our sample. The colors are all taken from 2000 s post burst trigger. The central wavelengths for the uvw1, b , and v filters are 2600, 4392, and 5468 Å, respectively. The error bar denotes the median errors for an individual measurement. Only bursts with detections in all three bands are represented.

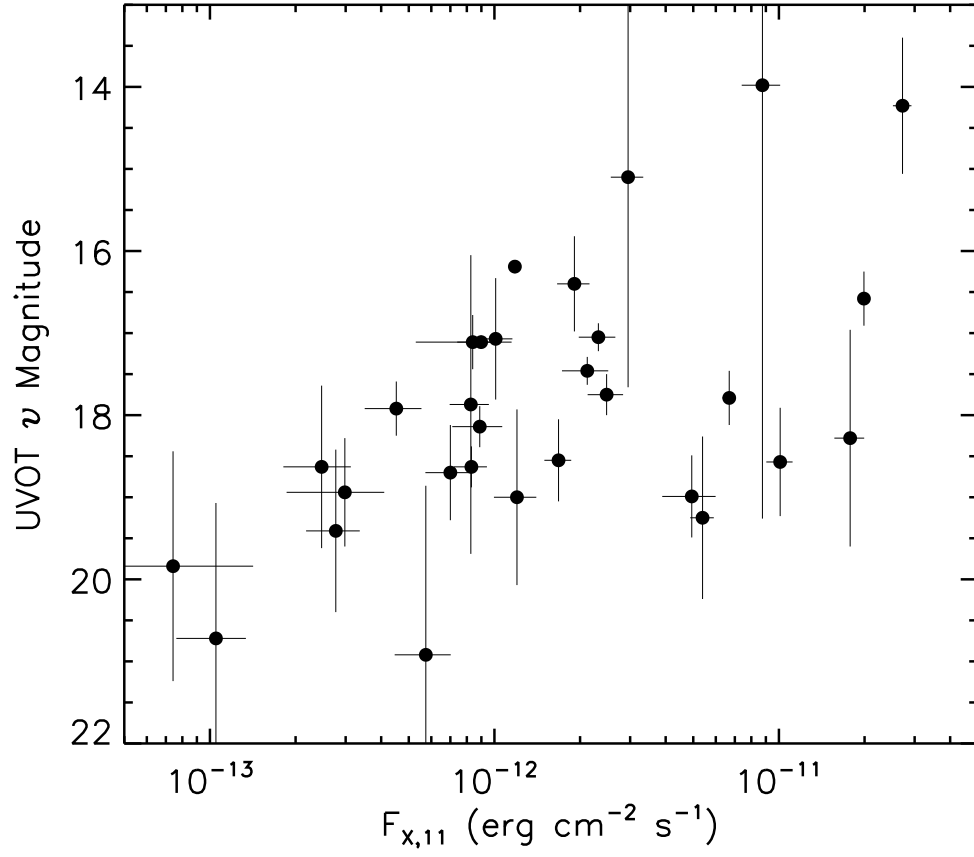


Fig. 15.— Comparison of the XRT flux at 11 hours ($F_{X,11}$) in the 0.3 – 10 keV band versus the UVOT magnitude in the v -band at 2000 s. Using the Spearman rank correlation, the data are strongly correlated ($p = 8.8 \times 10^{-4}$).

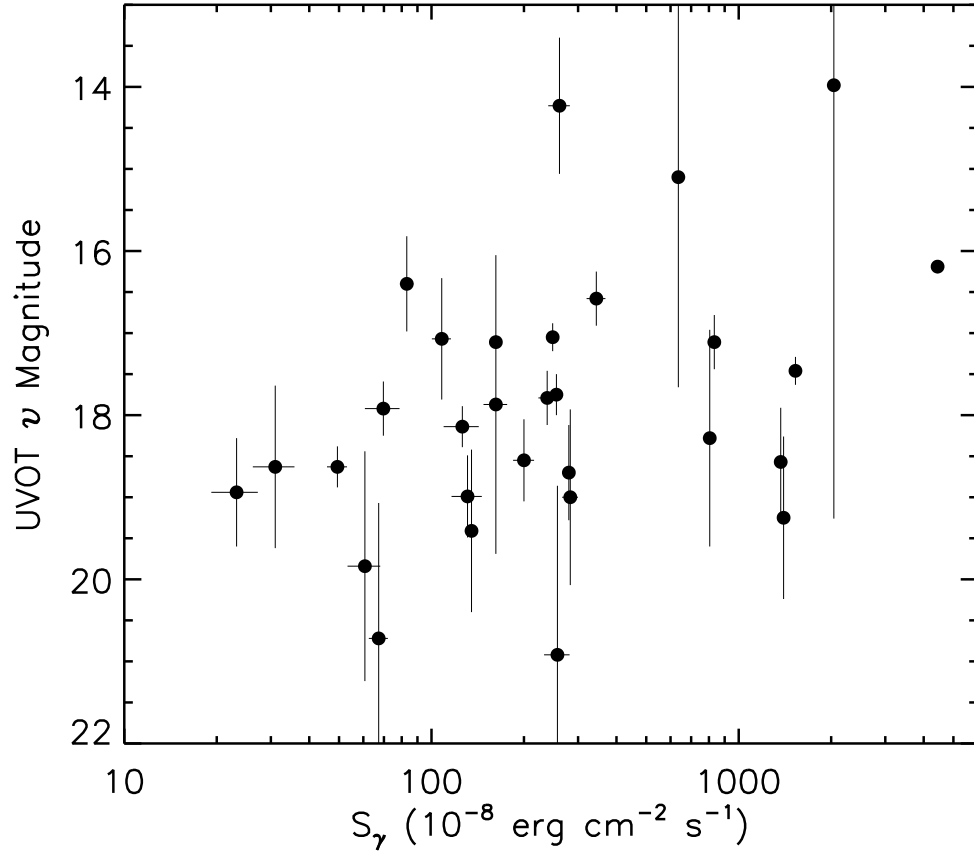


Fig. 16.— Comparison of the prompt BAT fluence (S_γ) in the 15 – 150 keV band versus the UVOT magnitude in the v -band at 2000 s. Using the Spearman rank correlation, the data are marginally correlated ($p = 0.0184$).

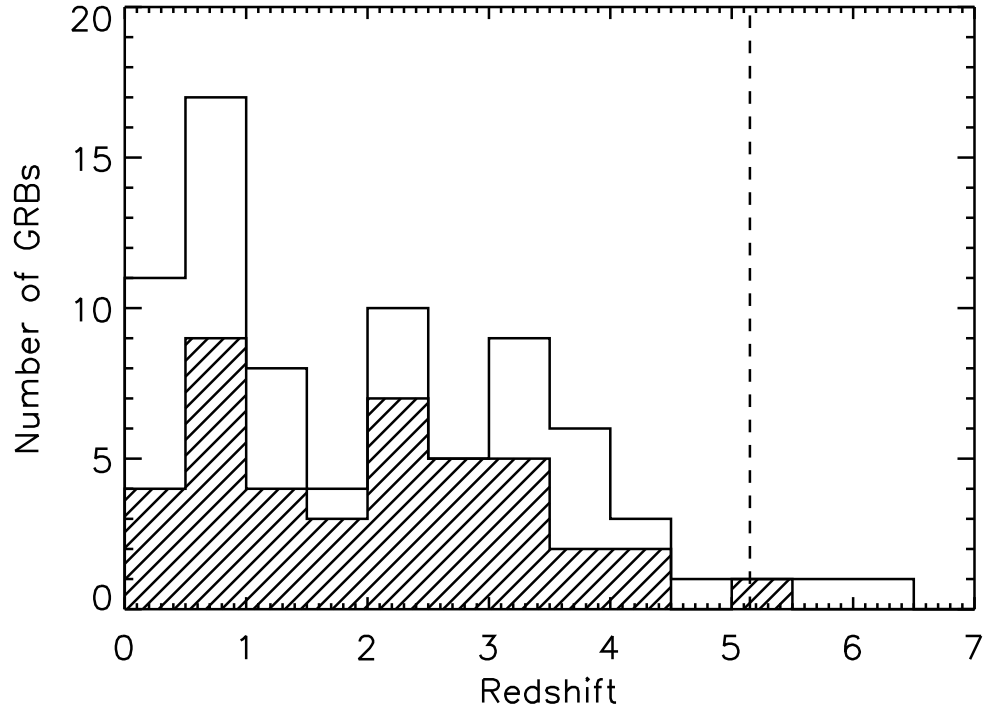


Fig. 17.— Distribution of measured burst redshifts. The measurements were made by ground based telescopes and not the UVOT. The shaded histogram is for the bursts with UVOT detections. The dotted line is the detection limit for UVOT